

**QUALITY ANALYSIS OF PETROLEUM COKES AND COALS
FOR EXPORT SPECIFICATIONS REQUIRED
IN USE OF SPECIALTY PRODUCTS AND UTILITY FUELS**

Jun M. Lee, James J. Baker, Daniel Murray, Robert Llerena, Jeffrey G. Rolle
A. J. Edmond Co.

1530 West 16th Street, Long Beach, CA 90813

Keywords: petroleum coke, coal, export quality

ABSTRACT

Quality of petroleum cokes and coals has been evaluated for export specifications required in use of specialty products and utility fuels. Various green and calcined cokes, produced at refineries in California, and coals for shipment are sampled at California and national ports, and analyzed by using ASTM Methods. Quality analysis reports include: proximate and ultimate analyses, metals, Btu, density, size distribution, hardgrove grindability, and other physical, chemical and mechanical properties. Some of recent analysis results from calcined petroleum coke produced for aluminum anode grade, green (raw) coke used in calcination, petroleum coke for high- and low-Btu fuel grade, low- and high-rank coals are compared and presented. QC/QA/SQC programs have been utilized for good precision and accuracy of data generated with acceptable repeatability and reproducibility.

INTRODUCTION

The A. J. Edmond Co. has over 30 years extensive experience specialized in analysis, testing and evaluation of petroleum cokes and coals for export specifications, which are used primarily as solid fuels in power plants and cement kilns and in other applications to produce specialty products, carbon anodes, metallurgical cokes, etc. Process development services currently provided include consulting, training, and process studies in production of calcined petroleum cokes for aluminum anode-grade. Quality of petroleum cokes was evaluated by Rolle, et. al [1,2], investigating the effects of metal impurities (vanadium, nickel and sodium) on the properties of cokes and anodes.

The quality of petroleum cokes produced by U. S. refineries has been affected by several major governing factors during the past decade from 1984 to 1993: (1) declining quality of crude oils, (2) coke production increase, (3) market demand and supply in liquid/solid fuels and exports, (4) specifications for end-use products, and (5) coking processes and calcination technology [3]. The average API gravity of crude oils declined annually by 0.17 degree/yr from 33 to 31; and the average sulfur content of crude oils increased by 0.029 wt%/yr from 0.88 to 1.21. As a result the coke production steadily increased by 51 % expecting continuous increase in the coming years, and the sulfur content of cokes is projected to increase from current average, 4.5 wt% to 5.5 wt% in future.

The U. S. coking capacity was fully utilized in 1993 having more than 100% coke production factor. The annual production was 78,430 tons/cd, of which 66% was exports (a major market demand) to Japan, Turkey, Italy, and other countries (total 44). The price of petroleum coke varies highly dependent upon its quality estimating in the range of \$19/ton for utility fuel-grade to \$550/ton for calcined super-premium needle coke. Anode-grade coke can vary from \$45/ton for green (raw) to \$200/ton for calcined.

The objective of this study is to evaluate the petroleum coke quality for export primarily based on recent analysis results from calcined petroleum coke produced for aluminum anode grade, green (raw) coke used in calcination, petroleum coke for high- and low-Btu fuel grade, and in addition the quality of low- and high-rank coals is evaluated.

SAMPLING AND PREPARATION

Representative samples of petroleum cokes and coals have been obtained from various refineries in California and storage facilities at numerous national ports. The auto sampler installed at the Long Beach port is sometimes used upon client's request for periodic routine sampling of blends for shipment. Laboratory samples are prepared for quality analysis following the procedures and principles in handling listed in the ASTM Methods D 346, D 2013 and D 2234, which are documented in the Quality Assurance Manual. Analysis samples are designated as refinery daily, weekly, monthly, M/V ship, QC/QA round robin, special test, etc. and stored for additional week, three or six months before disposal.

QUALITY SPECIFICATIONS FOR EXPORT

Petroleum cokes are produced at refineries using three different types of coking processes: delayed, fluid, and flexicoking. The delayed coker is mostly used at forty-nine U. S. refineries processing total 1.57 mm b/sd [3]. The other fluid coker and flexicoker are less utilized at a relatively smaller capacity (seven refineries and 0.2 mm b/sd). Coke products are classified as shot, sponge, (sometimes honeycomb), or needle coke depending on their chemical and physical characteristics. Shot coke is hard, having spherical form, and physically produced through precipitating asphaltenes; sponge coke is dull and black, having porous, amorphous structure, and is considered as a mixture of shot and needle cokes; and needle coke is silver-gray, having crystalline broken needle structure, and chemically produced through cross linking of condensed aromatic hydrocarbons during coking reactions[4].

Product grades and uses of green (raw) and calcined petroleum cokes

Green petroleum cokes are mostly used as utility fuels (about 73% for fuel-grade) in power generation and cement production including future developing projects of gasification IGCC and COG, and as feedstock (about 27%) for further upgrading calcination [5]. Uses of calcined cokes are: 71% for aluminum anode-grade, 9% for graphite electrodes, needle-grade, 8% for titanium dioxide pigments, 6% for recarburization of ductile iron products, and 6% for others (chlorine, phosphorous, silicon carbide, calcium carbide, etc.). Needle-grade calcined coke has three types, super-premium (SP), premium (P) and intermediate (I) depending on properties. Calcined petroleum cokes are used as reducing agent in production of titanium dioxide pigments because of extremely low ash and volatile content (6), and are further thermally treated at 2500 deg C to lower sulfur content to 0.03 wt% to meet specifications for recarburization (7).

Fuel-grade green coke

Depending on the location of refineries in the U. S. sulfur content of fuel-grade cokes varies; 2.25-2.60 wt% produced in Kansas and Oklahoma and 4.30-4.95 wt% in California, Louisiana Gulf Coast and Texas Gulf Coast. Typical ranges of coke properties for fuel-grade specifications are listed as follows:

13,000-15,000 Btu/lb
2.5-5.5+ wt% sulfur
200-400+ ppm vanadium
9-12 wt% volatile matter
0.1-0.3 wt% ash
100 HGI

Normally cokes are blended with coals at 10-20 % before burning in boilers because of their low volatile matter and high sulfur content. In use of cement kilns the addition of cokes can constitute up to 50 % of the fuel mixture and is carefully controlled conducting test burn due to detrimental effects of high sulfur and vanadium content to concrete quality [8]. Sulfur contamination can cause cement cracking and preheater plugging, and high vanadium content above 500 ppm can cause cement to lose strength.

Aluminum anode-grade calcined coke

Calcination process basically removes volatile matter, hydrogen and some of sulfur present in green cokes as a result increasing density and electrical conductivity suitable for use of carbon anodes in aluminum production. Typical ranges of calcined coke properties for aluminum anode-grade specifications are listed as follows [5,7-9]:

Property	Green	Calcined
wt% S	2.5	2.5 (1.7-3.0)
wt% ash	0.25	0.30 (0.1-0.3)
ppm V	150	200 (165-350)
ppm Ni	150	200(120-350)
wt% Si	0.02	0.02
wt% VM	10-12	<0.25
resistivity, microomega-m		950
real density, g/cu-cm		2.06
bulk density, g/cu-cm		0.80
coefficient of thermal expansion per deg C		2 x 10 to -6

Graphite needle-grade calcined coke

Feedstocks, needle coke precursors, are characterized by low API gravity, low asphaltene content, and a high degree of aromaticity [8]. Generally hydrocarbon streams are used with low sulfur content catalytic cracker slurry oils, tars derived from the thermal cracking of refinery gas oils, hydrodesulfurized catalytic cracker slurry oils, and coal tar pitches. Operating pressure and temperature of a coker are higher than other coking operations. The most important specification has been the coefficient of thermal expansion (CTE) as an indicator of the coke's structural alignment, which is related to the current-carrying capacity and mechanical integrity of resultant graphite electrodes. Typical ranges of calcined coke properties for graphite needle-grade specifications are listed as follows [7-9]:

Property	Green	Calcined (SP/P1)
wt% S	0.8	0.8 (0.3-0.8)
wt% ash	0.10	0.15 (0.03-0.2)
ppm V	10	10
ppm Ni		20-40
wt% Si	0.04	0.04
wt% VM	8	<0.25
resistivity, microomega-m		1100
real density, g/cu-cm		2.12 (2.12-2.15)
bulk density, g/cu-cm		0.88
coefficient of thermal expansion per deg C		0.3 x 10 to -6 (0.2-0.4 x 10 to -6)

Coal quality specifications

On-line coal quality analyzers are available for power plant monitoring and optimization resulting in lower operating costs [10]. Electric Power Research Institute (EPRI) developed coal quality impact model (CQIM) and coal quality evaluation system (C-QUEL). Coal quality is based on various complex properties such as heating value, ultimate analysis, ash content, moisture content, sulfur content, and mineral analysis. Key properties correlated for EPRI cause and effect relationships are ash, moisture, sulfur, silica, alumina, heating value, volatile matter, etc.

Typical ranges of coal properties analyzed at the A. J. Edmond Co. are listed in the following. Bituminous coal properties are obtained from M/V ship samples, and subbituminous coal properties are from western coal round robin samples.

Property (As-received)	Bituminous	Subbituminous
wt% moisture	6-10 (max. 10)	25-30
wt% ash	8-10	4-8
wt% volatile	36-41	30-35
wt% fixed carbon	42-47	30-35
Btu/lb	11,450-11,750	8,000-9,000
wt% sulfur (Ultimate, dry, wt%)	0.3-0.5	0.3-0.5
carbon	71-72.5	66-68
hydrogen	4.5-5.5	4.6-5.1
nitrogen	1.2-1.5	0.9-1.1
chlorine	0.01-0.03	
sulfur	0.4-0.5 (max. 0.7)	0.4-0.6
oxygen	10-12.5	17-20
(Mineral, wt% ash)		
silica	52-62	30-40
alumina	12-17	15-20
ferric oxide	3-7	3-6
titania	0.6-0.8	1-2
phosphorous pentoxide	0.2-0.8	
lime	7-14	15-25
manganese oxide	0.02-0.03	0.01-0.03
magnesia	1-3	3-6
barium oxide	0.04-0.11	
sodium oxide	0.5-4	1-3
potassium oxide	0.4-0.9	0.5-2

Property	Bituminous	Subbituminous
(Mineral, wt% ash)		
sulfur trioxide	5-7	10-15
Hardgrove Grindability Index	45-49	
ash fusion temperature, deg C		
IDT	+1,220	
HT	+1275	
FT	+1,340	
size 50 mm x 0	100%	
2 mm x 0	30% max.	

ANALYTICAL METHODS USED

Laboratory test methods using various advanced analytical instruments are described in the Quality Assurance Manual of A. J. Edmond Co. Primary analytical methods are summarized in the following.

Purpose	ASTM Method	Instrument
metals	D5600	ICP-AES
	D3682	ICP-AES, AA
	D5056	AA
sulfur	D4239	LECO
	D3177	PARR
	D1552	Dietert/LECO
	D5016	LECO
CHN	D5373	LECO
N	D3179	KJELDAHL
	ISO333	KJELDAHL
	D3286	PARR
Btu		PARR 1108, 1261, 1563
moisture	D3173	
ADL/RM	D3302, D4931	
volatile	ISO562, D3175, D4421	
ash	D4422, D3174	
VBD	D4292	
RD	D5004	
HGI	D5003, D409	
sieve	D5709, D293	

QC/QA/SQC PROGRAMS

Laboratory quality control (QC) program includes sample tracking and identification, sample preparation and analysis. Analytical tests are generally run within 24 hour period, however, some analyses of samples, i.e. moisture, sulfur, volatile, shot, etc. are completed in an hour, two hour or eight hour intervals in order to meet customer's requests and respond to any process changes. Information of analysis results is transferred through a Computer Data Base or simply by hand-written daily analytical reports. Statistical quality control (SQC) is performed by X and R control charts to assure good precision and accuracy of data generated with acceptable repeatability and reproducibility. Besides SQC trending or plotting of data, other notable quality assurance checks include use of calibration standards for elemental and metals analyses, daily instrument calibration, and check lists without any known standards. For quality assurance (QA) program in addition to the QC/SQC system, round robin samples of petroleum cokes and coals are analyzed routinely, monthly or as required, for further evaluation of the quality control results.

RESULTS FROM QUALITY TREND ANALYSIS

Quality of green petroleum coke (Figures 1-4)

Figure 1 shows sulfur content of green petroleum cokes obtained from fourteen refineries (designated as coke type A to N) and analyzed during the period of December 19, 1996 to February 20, 1997. Daily, weekly and monthly data are included for trend evaluation. Delayed cokes are A to L, fluid coke is M and type N is delayed coke used for calciner feedstock. A, B and C are best fuel-grade cokes with lowest sulfur content in the range of 0.8-1.6 wt% (average 1.0-1.2 wt%), while L has highest sulfur content of 4.2-6.0 wt%. Sulfur content of fluid coke M is 2.8-3.2 wt%.

In Figure 2 cokes A, B and C have highest heating values (15,500-15,800 Btu/lb), again best suited for fuel feedstock. Heating value of fluid coke M is lowest, 14,300-14,700 Btu/lb.

Figure 3 illustrates ash content varies in the range of 0.2 to 0.5 wt% except for coke N with 0.1 wt% ash, which is used for calciner feedstock.

Vanadium content of cokes significantly varies from 300 to 1600 ppm (Figure 4), depending on origin of production refinery and their usages. Good fuel-grade cokes A to E have vanadium content in the range of 300 to 600 ppm. Calciner feedstock coke N has 300-340 ppm vanadium.

Quality specifications of calcined petroleum coke (Figures 5 and 6)

Three different calcined petroleum cokes selected from M/V ship samples are compared in Figures 5 and 6. Most of our analytical data for these samples are within the specification limits for export. Sulfur content, vibrated bulk density (VBD), real density (RD), vanadium, nickel and sodium metal contents are plotted with actually measured, specification high and low values.

QC/QA/SQC programs

Figure 7 presents a SQC trend X-chart for sulfur content of green petroleum cokes (type A, B, C, L, M and N). For simplicity of presentation, only three data series show average, upper control limit (UCL) and lower control limit (LCL). All data are statistically controlled with two standard deviation interval at 95% confidence level.

SQC trend X-chart for metal contents (V, Ni and Na) of calcined cokes are plotted in Figure 8. These data were generated during the period of July, 1996 to February, 1997. Although the trend shows slightly increases in metal contents (about 20-30 ppm) in the latter part of the period, most of data are within the specification limits for export.

In January, 1997 a QA round robin sample of petroleum coke was analyzed for metal contents using PE Optima 3000 (ICP-AES). Test method was ASTM D 5600 performed with two different dissolution acids, 20% HCl and 4% HNO₃, respectively. Results of six analyses are summarized below.

Metal	Concentration, ppm		
	Average	Standard Deviation	ASTM RR Ranges
Si	61.2	25.6	19-94
	83.7 w/HCl	10.0 w/HCl	
	38.7 w/HNO ₃	4.5 w/HNO ₃	
Fe	46.5	1.8	17-94
V	402.8	4.4	24-59
Ni	168.2	3.5	17-23
Al	24.3	1.5	15-40
Ca	7.2	1.3	21-36
Na	34.5	6.1	10-31
Cr	0.5	----	----

With 20% HCl dissolution acid, silicon content of the coke is observed to be higher by 45 ppm than that with 4% HNO₃ dissolution acid. Other metal contents are similar with both acids. Good standard deviation values were obtained, and all are within ASTM repeatability and reproducibility (RR) ranges.

SUMMARY

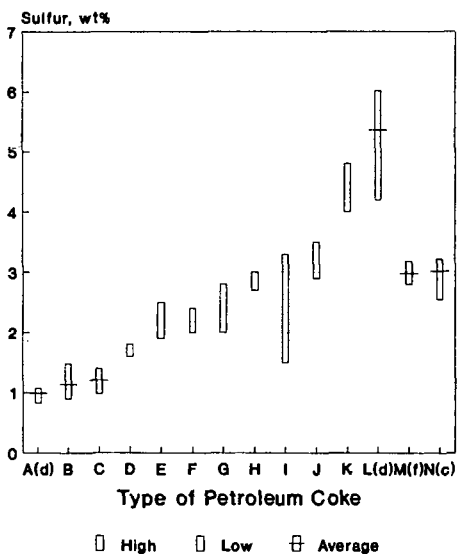
Quality of green (raw) and calcined petroleum cokes did not significantly change during the study period. Sulfur and metal contents (V, Ni and Na) of these cokes were statistically controlled, meeting the specification limits for export. In January, 1997 a slight increasing trend in metal contents (about 20-30 ppm) was observed. This increase may be speculated due to variety of reasons such as crude oil quality, coking and calcining process conditions, etc. QC/QA round robin results showed good repeatability and reproducibility in determination of metals present in petroleum coke by ICP-AES.

Future studies of interest include: expansion of data base beyond the current study period, coal quality analysis for power plant fuels and metallurgical cokes, sampling and sample preparation, problem solving in QC/QA, and quality impacts on end-use products (aluminum anode, graphite electrode, TiO₂, recarburization, etc.).

REFERENCES

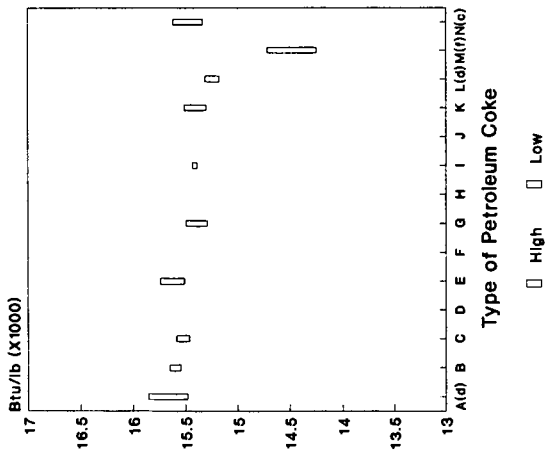
1. J. G. Rolle, et. al., *Light Metals 1997*, 489-495, 126th TMS Annual Meeting, Orlando, FL, Feb. 9-13.
2. J. G. Rolle and Y. K. Hoang, *Light Metals 1995*, 124th TMS Annual Meeting, Las Vegas, Feb. 12-16.
3. E. J. Swain, *Oil & Gas Journal*, Jan. 2, 1995, 33-39; Jan. 9, 1995, 37-42.
4. N. P. Lieberman, *Oil & Gas Journal*, Mar. 27, 1989, 67-69.
5. R. E. Dymond and B. H. Spector, *Light Metal Age*, Feb. , 1992, 34-38.
6. W. M. Goldberger, et. al., *Petroleum Derived-Carbons*, ACS Symposium Series 303, 1986, Ch. 15, 200-214, (Edited by J. D. Bacha, et. al.).
7. *Ullmann's Encyclopedia of Industrial Chemistry*, Volume A20 and A27 (1986).
8. E. J. Swain, *Oil & Gas Journal*, May 20, 1991, 49-52.
9. *Kerk-Othmer Encyclopedia of Chemical Technology*, Volume 4, 4th Ed., Carbon, 956 (1992).
10. D. Mitas, et. al., *Power Engineering*, May, 1991, 29-32.

Figure 1. SULFUR CONTENT OF GREEN COKE



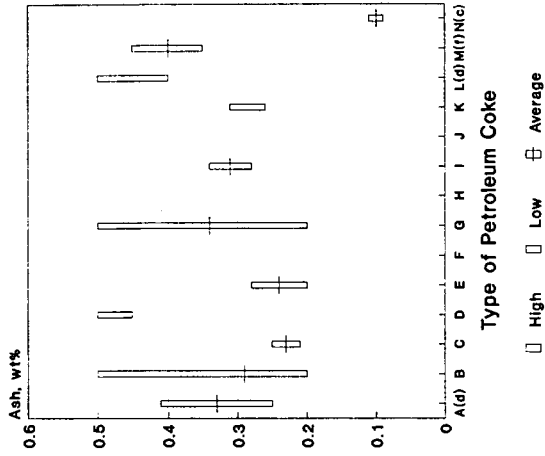
Period: 12/19/96-02/20/97

Figure 2. CALORIFIC VALUE OF GREEN COKE



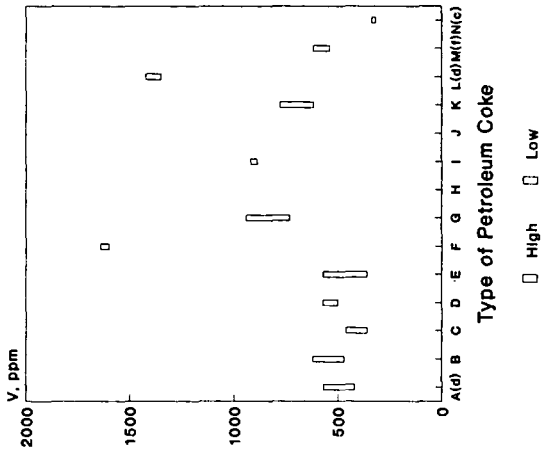
Period: 12/19/96-02/20/97

Figure 3. ASH CONTENT OF GREEN COKE



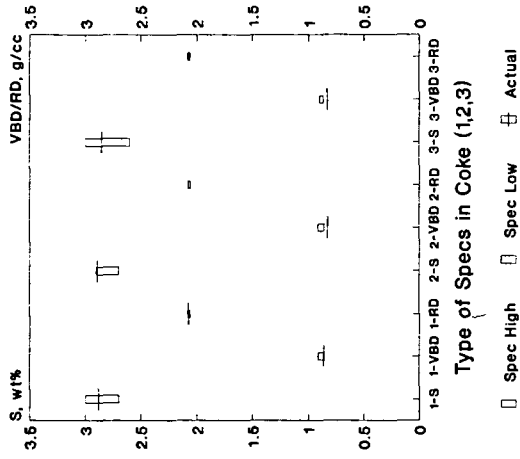
Period: 12/19/96-02/20/97

Figure 4. VANADIUM CONTENT OF GREEN COKE



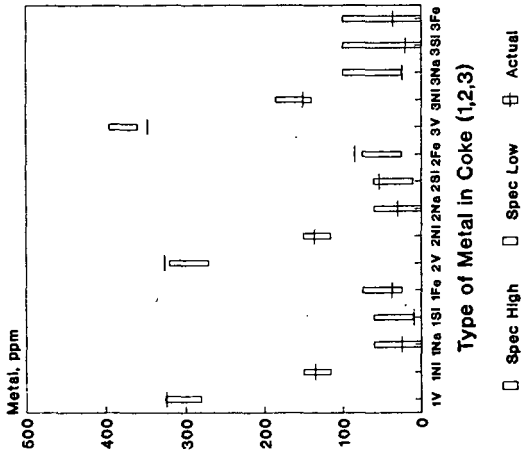
Period: 12/19/96-02/20/97

Figure 5. QUALITY SPECS OF CALCINED COKE
Aluminum Anode-Grade



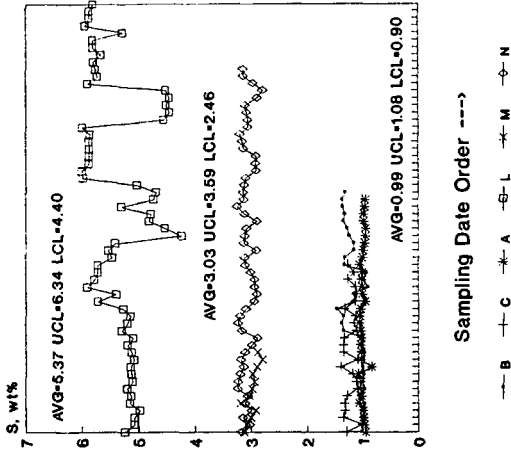
Period: 12/19/96-02/20/97

Figure 6. METAL CONTENT OF CALCINED COKE
Aluminum Anode-Grade



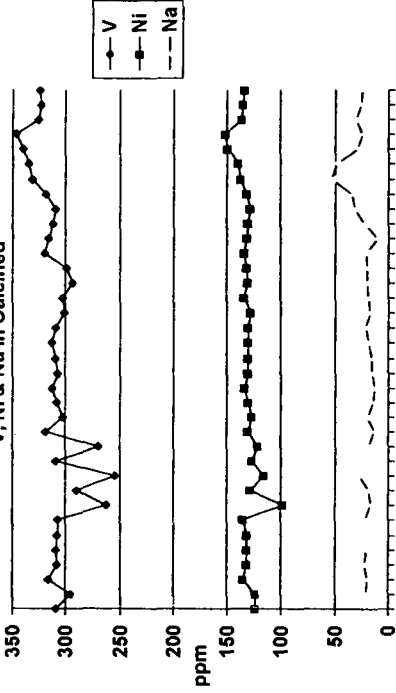
Period: 12/18/86-02/20/87

Figure 7. QC TREND CHART
Sulfur Content of Coke



Period: 12/18/86-02/20/87

Figure 8. QC TREND CHART
V, Ni & Na in Calcined



Sampling Date Order → (Period: 7/96-2/97)

V: AVG=308.9 UCL=347.1 LCL=270.7
 Ni: AVG=130.9 UCL=147.9 LCL=113.9
 Na: AVG= 22.5 UCL= 40.7 LCL= 4.3

SMALL ANGLE NEUTRON AND X-RAY SCATTERING STUDIES OF CARBONS PREPARED USING INORGANIC TEMPLATES

Giselle Sandí, Pappannan Thiyagarajan[†], Randall E. Winans, and Kathleen A. Carrado
Chemistry and [†]Intense Pulsed Neutron Source Divisions
Argonne National Laboratory, Argonne, IL 60439

ABSTRACT

Small angle neutron (SANS) and X-ray (SAXS) scattering analyses of carbons derived from organic-loaded inorganic template materials, used as anodes in lithium ion cells, have been performed. Two clays were used as templates to load the organic precursors, pillared montmorillonite (PILC), a layered silicate clay whose sheets have been permanently propped open by sets of thermally stable molecular props, and sepiolite, a natural channeled clay. Five different organic precursors were used to load the PILC: pyrene, styrene, pyrene/trioxane copolymer, ethylene and propylene, whereas only propylene and ethylene were used to load sepiolite. Pyrolysis took place at 700 °C under nitrogen. Values such as hole radius, fractal dimension, cutoff length and density of the final carbons will be compared as a function of the clay and carbon precursors.

INTRODUCTION

In these studies, SANS and SAXS scattering techniques are used to obtain information concerning the hole radius, fractal dimension, cutoff length and density of carbons and their precursors, prepared using inorganic pillared templates. These carbons have been tested in electrochemical cells as anodes in lithium secondary batteries and proved to deliver high specific capacity (a measure of the power in mAh/g) and excellent performance in terms of the number of cycles runs (1,2). Preliminary results suggested that these carbons contain holes whose diameter is approximately the same as the Al₁₃ pillar, thus facilitating the lithium ion diffusion. It is one of our goals to determine the distribution of the carbon within the pillared clay before and after the heating process and upon removal of the pillared clay by acid treatment.

A critical feature of SANS and SAXS scattering methods is their potential for analyzing the inner structure of disordered systems. Their application is a unique way of obtaining direct information on systems with a random arrangement of density inhomogeneities in a colloid-size range. The signal measured in SANS is the intensity of scattered neutrons as a function of the scattering angle. Since the scattering angle θ is related to the wave vector of the scattered radiation according to:

$$q = \frac{2\pi}{\lambda} |s - s_0| = \frac{4\pi}{\lambda} \sin \frac{\theta}{2} \quad (1)$$

where s and s_0 are the unit vectors in the direction of the incident and scattered radiation, it is customary to express the scattering intensity as a function of the wave vector q .

The amplitude of the scattered radiation is given by:

$$A(q) = b \sum_{k,l} e^{-iq \cdot r_{kl}} \quad (2)$$

where b is the scattering length of one atom and r_{kl} is a vector describing the distance between atom k and l . The intensity of the scattered radiation $I(q)$ is proportional to the square of this amplitude. The product of wave vector q and the distance between two scattering centers r_{kl} determines the phase difference between two scattered waves. The smaller the scattering angle, i.e., the smaller the q value, the larger the particle size can be from which emanates scattered radiation before a phase difference that leads to destructive interference is established. The total scattering signal reflects an average measure of the particle size and geometry (3). Since the high- q range of the scattering function results from the smallest features of the scattering particles, the inverse power terms describe the external surface of the particles, and the exponent depends entirely on the structure of this surface.

For porous materials, depending on the geometrical arrangement of the filled or the void space, the power law that describes the mass scaling may have an exponent of less than three. In the most general case the scaling law is given by:

$$M(r) \propto r^{d_f} \quad (3)$$

where the d_f is called the Hausdorff dimension or fractal dimension and can assume noninteger values. It describes how the mass of the cluster increases with its linear dimension r . While a material may appear perfectly regular and three dimensional on the scale of a centimeter it may scale in a fractal way on the scale of a nanometer. Diffraction experiments probe the density correlations on length scales that correspond to the inverse momentum transfer q^{-1} , and since the intensity per particle scales with the correlated mass in the probing volume, it is expected that the intensity scales as q^{-d_f} .

SAXS probes scattered wave vectors q ranging from 10^{-4} to 10^1 \AA^{-1} , where the scattered wave vector is defined as in equation 1. Scattered intensities reflect a correlation in X-ray scattering length density on length scales between 10 and 10^4 \AA . For porous materials consisting of a void and a solid phase, the difference in scattering length density is approximately equal to the scattering length density of the solid phase.

EXPERIMENTAL

The synthesis of the calcined pillared clays (PILCs) has been described in detail elsewhere (1,2). The calcined PILC was loaded with five different organic precursors using the procedures summarized as follows. For pyrene, the pillared clay is stirred in a 0.1 M solution of pyrene in benzene at room temperature overnight. Liquid styrene was heated under a nitrogen flow in a vacuum system. The styrene vapor was carried to a round bottom flask containing the PILC. The PILC was stirred as a solid phase and heated to 150°C . Trioxane was heated to 70°C . Pyrene was added to the reaction vessel once the trioxane was completely melted. PILC was then added to the solution and stirred. The reaction was catalyzed by addition of few drops of 0.1 M HCl. The excess trioxane and pyrene mixture was washed away with toluene before pyrolysis. The pyrolysis of the above samples took place in stainless steel tubes purged with nitrogen for several minutes. The tubes were sealed and heated to 700°C for 4 hours. Ethylene and propylene were loaded in the gas phase, where the loading and the pyrolysis processes were done in one step. Here, a three-zone furnace was used. Quartz boats containing PILC or sepiolite were placed within a quartz tube. The tube was initially flushed with nitrogen for about 3 hours. After that period of time, the gas was switched to propylene or ethylene and the gas flow was kept about $5 \text{ cm}^3/\text{min}$. The temperature of the oven was gradually increased from room temperature (about $5^\circ\text{C}/\text{min}$) to 700°C . The oven was then held at that target temperature for 4 hours.

The clay from the loaded/pyrolyzed PILC or sepiolite was removed using HF, rinsed to neutral pH and refluxed with concentrated HCl for 2 hours. The sample was washed with distilled water until the pH was > 5 to ensure that there was no acid left. The resultant carbon was oven dried overnight at 120°C .

X-ray powder diffraction (XRD) patterns of clay precursors and carbons were determined using a Rigaku Miniflex, with Cu K_α radiation and a beryllium solid-state detector at a scan rate of $0.5^\circ/2\theta/\text{min}$.

SANS experiments were conducted at the Intense Pulsed Neutron Source at Argonne National Laboratory. The powders were held in 1mm path quartz cells. The incident neutron spectrum is supplied by a cold moderator. The wavelength of the scattered neutrons range between 0.5 and 14 \AA , binned into 67 wavelength channels with 5% wavelength spread in each channel. This instrument uses a BF_3 detector, and the scattered neutrons are detected by a $20 \times 20 \text{ cm}^2$ ^3He area detector with 64×64 spatial channels. The q range covered is $0.005\text{-}0.35 \text{ \AA}^{-1}$. The measurements took about two hours per sample. SAXS data were obtained at the Center for Micro-Engineered Materials, University of New Mexico. Both a Bonse-Hart and pin-hole instrument were used, resulting in a q range of $0.0002\text{-}0.8 \text{ \AA}^{-1}$.

RESULTS AND DISCUSSION

Figure 1 shows SANS data for PILC, PILC loaded with pyrene before pyrolysis and the carbon obtained after pyrolysis at 700°C and removal of the clay matrix. Scattering curves are nearly identical for the PILC and the loaded clay, indicating no appreciable structural changes of the pillared clay upon organic incorporation. Both the pillared clay and the loaded pillared clay exhibit a hump in the middle- q region that suggests a high degree of aggregation. The scattering

in the middle- q region of the carbon sample did not show the aggregation feature observed in the PILC and PILC/pyrene.

Figure 2 shows SANS data for five carbons derived from PILC and different organic precursors. Note that for the carbons derived from trioxane/pyrene copolymer, ethylene and propylene, a certain degree of aggregation is observed at the middle- q region. The low and high q regions are very similar. These data were evaluated as described by Freltoft *et al.* (4) to fit the experimental data in terms of the adjustable parameters d_f (fractal dimension), r_0 (cluster size) and ξ (cutoff length). It is not possible to discriminate between voids and clusters, thus, r_0 represents an average of both voids and clusters. ξ is related to the macroscopic density of the material, and d_f represents the particle distribution; it is a description of the geometrical arrangement of the particles in a cluster. A perfectly layered material such as graphite under well dispersed, conditions would exhibit $d_f=2$.

Table I summarizes the above parameters calculated for carbons and their precursors. The fractal dimensions for the carbon are similar to those calculated for the PILC, indicating that there is some layering in these disordered systems. Furthermore, r_0 of the holes for the carbonaceous materials range from about 4 to 8 Å, the largest radius corresponding to the carbon derived from PILC/pyrene. SAXS data of a carbon sample prepared from PILC/pyrene is shown in Figure 3. In the middle- q range the scattering intensity is characterized by a fractal dimension of 2.56, whereas at low q the fractal dimension corresponds to 3.88, which suggest that they have a small amount of roughness.

Another clay template used in the preparation of holey carbons is called sepiolite. It has the general structure $\text{Si}_{12}\text{Mg}_9\text{O}_{30}(\text{OH})_6(\text{OH}_2)_4 \cdot 6\text{H}_2\text{O}$ (5). It is a clay that does not have to be pillared since it contains a channeled structure. Preliminary results using pyrene as the organic precursor demonstrated that some carbon is incorporated into the clay. However, smaller molecules such as propylene or ethylene may be incorporated at a faster rate. Figure 5 shows an X-ray powder diffraction (XRD) of the carbon synthesized by incorporating propylene within sepiolite in the gas phase. The broad peak corresponds to the 002 reflection and is indicative of a disordered system. Further characterization of this carbon by SANS, SAXS and electrochemical testing is in progress.

CONCLUSIONS

Analysis of SANS and SAXS data of carbons synthesized using clays as templates show that they contain holes with a radius range from 4 to 8 Å. These holes are accessible to lithium ions when the intercalation process takes place in a lithium secondary battery. The values of the fractal dimension for the carbons are similar to those found for the clays, suggesting that there is some layering in the disordered system.

ACKNOWLEDGMENTS

The help in acquiring SANS data from Mr. D. Wozniak and Dr. C. Y. Ku, from the Intense Pulsed Neutron Source at Argonne National Laboratory, is greatly appreciated. This work was performed under the auspices of the Office of Basic Energy Sciences, Division of Chemical Sciences, U.S. Department of Energy, under contract number W-31-109-ENG-38.

REFERENCES

1. G. Sandí, R. E. Winans, and K. A. Carrado, *J. Electrochem. Soc.*, **143**, L95 (1996).
2. G. Sandí, K. A. Carrado, R. E. Winans, J. R. Brenner and G. W. Zajac, *Mater. Res. Soc. Symp. Proc., Macroporous and Microporous Materials* **431**, 39 (1996).
3. J. R. D. Copley, *J. Appl. Cryst.*, **21**, 639 (1988).
4. T. Freltoft, J. K. Kjems, and S. K. Sinha, *Physical Review B* **33**, 269 (1986).
5. J. M. Thomas, in *Intercalation Chemistry*, M. S. Whittingham, and A. J. Jacobson, Editors, p. 61, Academic Press, New York (1982).

Table I: Experimental parameters calculated from SANS data.

Sample	$r_g/\text{\AA}$	$\xi/\text{\AA}$	d_f
PILC	3.70	876	2.469
Carbon from PILC/pyrene	7.66	1080	2.660
Carbon from PILC/styrene	6.60	148	2.650
Carbon from PILC/ethylene	4.00	143	2.690
Carbon from PILC/propylene	4.30	534	2.880
Carbon from PILC/trioxane/pyrene	1.40	NA	2.930

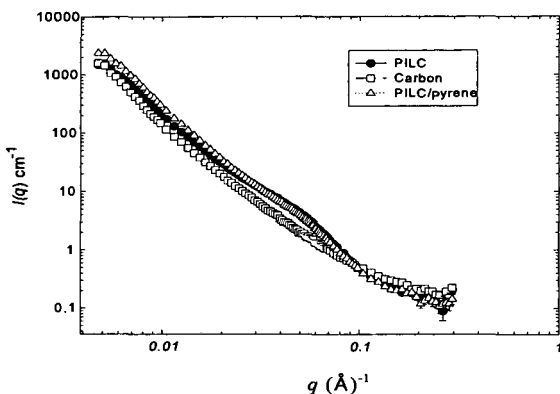


Figure 1: $\log I$ vs $\log q$ plot of the small-angle neutron scattering for (●) PILC, (Δ) PILC/pyrene and (□) carbon obtained after pyrolysis and clay removal.

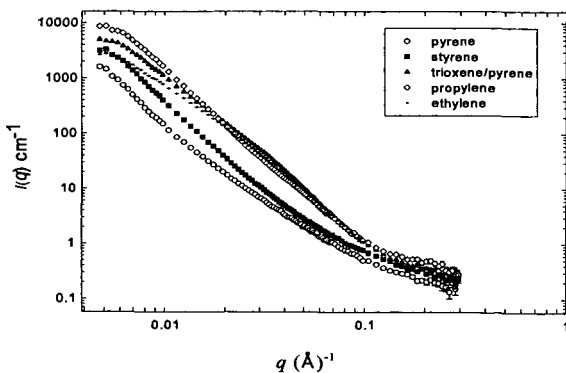


Figure 2: $\log I$ vs $\log q$ plot of the small-angle neutron scattering for carbon samples prepared using PILC and different organic precursors. (○) pyrene, (■) styrene, (▲) trioxane/pyrene, (◇) propylene and (◊) ethylene.

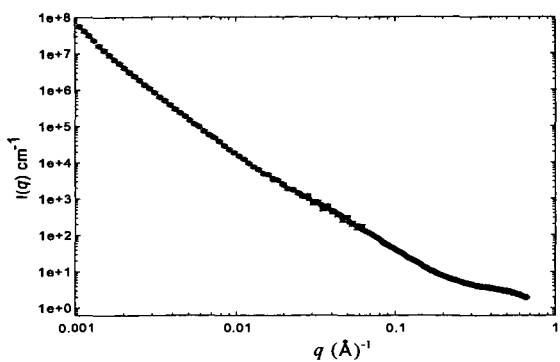


Figure 3: $\log I$ vs $\log q$ of the small angle X-ray scattering of a carbon sample derived from PILC/pyrene.

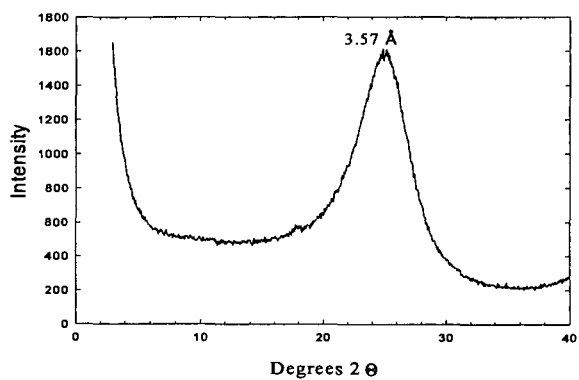


Figure 4: XRD of a carbon derived from sepiolite/propylene.

FRACTAL ANALYSIS OF GRANULAR ACTIVATED CARBONS USING ISOTHERM DATA

Nasrin R. Khalili, and Minzi Pan, Department of Chemical and Environmental Engineering, Illinois Institute of Technology, Chicago, IL 60616
Giselle Sandi, Chemistry Division, Argonne National Laboratory, Argonne, IL 60439

INTRODUCTION

Utilization of adsorption on solid surfaces was exercised for the first time in 1785. Practical application of unactivated carbon filters, and powdered carbon were first demonstrated in the American water treatment plant, and a municipal treatment plant in New Jersey, in 1883 and 1930, respectively. The use of activated carbon became widespread in the next few decades. At present, adsorption on carbons has a wide spread application in water treatment and removal of taste, odor, removal of synthetic organic chemicals, color-forming organics, and disinfection by-products and their naturally occurring precursors.

Along with the application of adsorption, the theoretical study has been more and more profound. The concept of adsorption isotherm introduced to specify the equilibrium surface concentration of adsorbate on adsorbent as a function of bulk concentration of adsorbate. The three famous mathematical models Langmuir, BET, and Freundlich were developed to describe the adsorption isotherm for single adsorbates. Langmuir adsorption isotherm describes equilibrium between surface and solution as a reversible chemical equilibrium between species. Adsorbent surface is considered to be made up of fixed individual sites where molecule of adsorbate, may be chemically bounded. Each site is assumed to be capable of binding at most one molecule of adsorbate. Langmuir model allows accumulation only up to a monolayer while the total amount of mass adsorbed is assumed to approach a saturating value when concentration becomes very large. Since both BET and Freundlich models were used in this study, settings of these models are presented.

The BET adsorption isotherm, extended the Langmuir model from a monolayer to several molecular layers. Model assumes that above the monolayer, each additional layer of adsorbate molecules is in equilibrium with the layer below it. Therefore layers of different thickness are allowed to co-exist. Under this circumstances, the process of sorbing a new layer of adsorbate onto old layers is assumed to be identical to the process of condensing adsorbate from solution to solid or liquid. The resulting isotherm is known to have the form of:

$$\frac{V}{V_m} = \frac{cX}{1-X} \sum_{n=1}^{\infty} B_n \left(\frac{1-(n+1)X^n + nX^{n+1}}{1+(c-1)X - cX^{n+1}} \right) \quad (1)$$

In this model, V is the volume of adsorbate per mass of adsorbent at equilibrium, V_m is the volume of monolayer adsorbate per mass of adsorbent, c is a dimensionless constant that is related to the difference in free energy between adsorbate on the first and successive layers, n represents the number of layers adsorbed, B_n is the fraction of adsorbent surface that is covered by n layers of adsorbate, and X is the value of p/p_0 (p = equilibrium partial pressure of adsorbate, p_0 = the saturated vapor pressure). The parameter B_n introduces the unsimilarity between the area at the n th layer and adsorbent surface, for adsorbents with uneven surfaces. Traditionally, since B_n is difficult to be determined, it is assumed that all layers have the same surface area as that of the adsorbent, and therefore an infinite number of layers of adsorbate would be expected. The summation in the above equation has a single term with $B_n = 1$ for $n = \infty$. Recently using fractal theories parameter B_n has been estimated for fractal surfaces.

For low concentration systems ($X \ll 1$) the BET model can be simplified as:

$$\frac{X}{V(1-X)} = \frac{1}{V_m c} + \frac{c-1}{V_m c} X \quad (2)$$

The BET adsorption isotherm suggests that surface concentration reaches a plateau as the monolayer is filled, then increases proportional to increase in p . Langmuir and BET models incorporate an assumption that the energy of adsorption is the same for all surface sites and not dependent on degree of coverage. In reality, the energy of adsorption may vary because real surfaces are heterogeneous.

Another isotherm model which has been used widely is the Freundlich adsorption isotherm. This model attempt to account for energy of adsorption, assuming that, the frequency of sites associated with a free energy of adsorption decreases exponentially with increasing free energy. The Freundlich isotherm has the form of $q = k C^{1/n}$, where k and n are constants. In this model the surface concentration of adsorbate does not approach a saturating value as C increases, since there are always surface sites with higher free energies of adsorption to fill. The Freundlich

isotherm is very widely used to fit observed data empirically even when there is no basis for its underlying assumptions.

Fractal Dimension

Fractal geometry is a mathematical tool for dealing with complex systems that have no characteristic length scale. The scale-invariant systems, are usually characterized by noninteger or "fractal" dimensions. The concept of fractal dimension, d , can be expressed as how the mass $M(L)$ changes with the linear size L of the system with uniform density. In fractal systems, a smaller part of the system of linear size bL ($b < 1$), the $M(bL)$ is decreased by a factor of b^d , such as $M(bL) = b^d M(L)$. Simply we can assume that $M(L) = AL^d$, with A being constant.

The Koch Curve is one of the most common deterministic fractals. In Koch curve, by each iteration the length of the curve is increased by a factor of $4/3$. The mathematical fractal then is defined in the limit of infinite iterations, $n \rightarrow \infty$, where the total length of the curve approaches infinity. If the linear size is decreased by a factor of $b=1/3$, the total length (mass) of the curve will be decreased by a factor of $1/4$ (i.e., $M(\frac{1}{3}L) = \frac{1}{4}M(L)$). Therefore, it can be assumed that $1/4 = (1/3)^d$, and $d = \log 4 / \log 3$. Such non integer dimensions are called "fractal dimension" and those objects described by a fractal dimension are called fractals.

Applying fractal dimension theory, one can derive different methods to measure the dimension of a fractal surface. In the traditional adsorption theories, the adsorbent's surface is simplified to be a locally flat surface, giving $d=2$. But many adsorbents' surfaces are sufficiently porous and irregular. For example, the radius of micropores in activated carbon can be smaller than 1 nm, while that of the macropores can be bigger than 25 nm. For such surfaces, a minor changes in the size of adsorbate molecules can result in a great change for monolayer coverage.

The geometrical complexity of the surface of many irregular adsorbents, such as activated carbons and wood suggests that, surfaces structure of these adsorbents can be easily described according to the fractal theory. The fractal dimension "d" then would be a measure of adsorbent's surface irregularity. Recent studies showed that, values of "d" that expresses the degree of complexity of surface and/or porous structure, fall in the range of 2-3, representing extremely heterogeneous surfaces (Pfeifer et al., 1983, Jaroniec and Kruk, 1997). A specific value of "d" demonstrate self similarity, showing that any section of surface unfolds into m^d similar sections upon m -fold magnification. A dimension higher than 2 implies that any monolayer on a surface with $d > 2$ correspond to a three dimensional bulk rather than a two dimensional film. Under this condition, the number of adsorption sites within distance L from any fixed site grows as L^d .

Many methods have been developed in order to obtain "d" on the basis of adsorption, mercury porosimetry, scanning electron microscopy, and small-angle X-ray and neutron scattering measurements (Jaroniec and Kruk, 1997). Among those, adsorption method play an important role. Some of the fractal oriented adsorption theories are simple and convenient since they require only one complete adsorption isotherm for a given solid to calculate the value of "d".

This paper presents the results of a study conducted to investigate the extent of association between surface fractal dimension and adsorption capacity of a group commercial and disorder carbons, using BET isotherm data and a model proposed by Segars et al., 1996.

STUDY APPROACH

The purpose of this study was to: a) use an appropriate model and gas phase isotherm adsorption data to estimate fractal dimensions of a range of carbons with different surface structure, and b) propose a model that can predict adsorption capacity of carbons in a single component liquid phase system, using estimated fractal dimensions.

Study was conducted in four steps: 1) using volumetric isotherm test (BET test), adsorption-desorption isotherms of nitrogen on selected carbons were determined, 2) using a model proposed by Segars et al., 1996, and gas phase isotherm data, fractal dimensions and other specific surface parameters were evaluated, 3) liquid phase isotherm data were determined using a single component liquid phase system containing phenanthrene-9-¹⁴C, and 4) a modified adsorption model that relates liquid phase adsorption capacity to the surface dimension "d" was proposed. While liquid phase modeling is in progress, the obtained results of fractal analysis are presented.

RESULTS

Volumetric (gas phase) isotherm data were determined for two granular activated carbons (GAC 1240 and Sorbonorite 4), and four disorder carbons synthesized at the Argonne National Laboratory, using clay as templates (carbons # 1 to 4). An example of the adsorption-desorption isotherms for these carbons are presented in Figures 1. As it is shown adsorption type II and III were observed for these carbons. Using volumetric isotherm data and modified BET model proposed by Segars et al., 1996 (this model introduces the fractal dimension to the adsorption isotherms), important parameter B_n in BET model was estimated as follows:

$$B_n = \left(\frac{r}{L}\right)^{d-d_{n+1}} - \left(\frac{r}{L}\right)^{d-d_n}, \text{ where :}$$

$$d_{n+1} = [1 - LN\left(\frac{r}{L}\right)] - \sqrt{[1 - LN\left(\frac{r}{L}\right)]^2 + 2[d_n * LN\left(\frac{r}{L}\right) + (d-2) * LN2 - LN(3-d_n)]}$$

The fitting parameters to the model were the gas phase isotherm adsorption data. The pressure p was ranging from 0 to p_0 and parameter "r" was the size of adsorbed molecule. The computer simulation predicted parameters : d , r/L , V_m , c , and the maximum number of adsorbed layer, N .

The results of modeling simulation are provided in Table 1. As it is indicated fractal dimension of commercial carbons were above 2.5, endorsing a non- flat surface structure for these adsorbents. However the modeled "d" for disorder carbons were about 2.1 representing relatively flat surfaces. For comparison, the V_m values estimated by the traditional BET model are also included in the Table 1. The estimated standard deviation for V_m indicated that model can accurately predict the volumetric isotherm data, using estimated parameters. Figures 2, shows examples of the modeled (line) and measured isotherm curves for these carbons. In general results of modeling showed that modified BET model can accurately estimate gas phase adsorption isotherms, and adsorption for these carbons matches type II adsorption isotherm better than type III.

The liquid phase adsorption isotherms were evaluated for carbons from measured concentration of Phenanthrene-9-¹⁴C at equilibrium, using Freundlich isotherm model ($q = kC^{1/n}$). Table 2 shows calculated adsorption capacity k , and degree of bonding , $1/n$ for all six carbons. The adsorption capacity of disorder carbons was much lower than commercial carbons. The liquid phase adsorption data were in a good agreement with the results of fractal modeling, suggesting that carbons with fractal surface have higher adsorption capacity in liquid phase systems.

CONCLUSION

Using a modified BET isotherm model and volumetric isotherm data, fractal dimensions of two commercial carbons, GAC 1240 and Sorbonorite 4, were estimated. The fractal dimension "d" for these carbons were about 2.7 and 2.6 respectively. The estimated monolayer volumes for these two carbons were 25-27 % larger than the volumes determined by BET. The disordered (synthesized) carbons showed a surface dimension of near 2, representing a flat surface. The monolayer volumes for these four disordered carbons were similar to the results of BET analyses. Liquid phase isotherm data showed a much higher adsorption capacity for commercial carbons with fractal dimension than disorder carbons. Development of a model that can predict liquid phase adsorption capacity of these adsorbents as a function of their surface dimensions is in progress.

ACKNOWLEDGMENT

Part of this work was performed under the auspices of the Office of Basic Energy Sciences, Division of Chemical Sciences, U.S. Department of Energy, under contract number W-31-109-ENG-38.

REFERENCES

- Jaroniec, M., Kruk, M., Olivier J. 1995. Verification of selected relationships for Fractally Porous Solids by Using Adsorption Isotherms Calculated from Density Functional Theory. *Surface Science* 342, L1127-L1130
- Jaroniec, M., Kruk, M. 1997. Fractal Analysis of Composit Adsorption Isotherms Obtained by Using Density Functional Theory Data for Argon in Slitlike Pores. *Langmuir*, 13, pp 1031-1035
- Pfeifer, P., Anvir, D. 1983. Chemistry in Noninteger Dimensions Between Two and Three.I. Fractal Theory of Heterogeneous Surfaces. *J.Chem.Phys.* 79(7), pp 3558-3565
- Segars R. and Piscitelle, L. 1996. Verification and Application of a New Adsorption Model for Fractal Surfaces. *Mat. Res. Soc. Symp. Proc.* Vol 407, pp 349-354

Table 1. Estimated Surface Parameters Using Modified BET Model

Adsorbent		d	r/L	C	N	V _m	S
Sorbonorite 4	fractal	2.7	0.1	100	11	405	4.24
	B.E.T.	--	--	99	--	293	
GAC 1240	fractal	2.6	0.1	250	45	282	2.03
	B.E.T.	--	--	67	--	210	
Carbon #1	fractal	2.1	1E-5	90	90	48	21.1
	B.E.T.	--	--	107	--	55.5	
Carbon #2	fractal	2.2	1E-5	31.2	45	1.39	0.25
	B.E.T.	--	--	23.8	--	1.36	
Carbon #3	fractal	2.45	0.01	400	95	115	10.6
		--	--	111	--	100	
Carbon #4	fractal	2.1	1E-6	90	90	6.57	3.08
	B.E.T.	--	--	406	--	6.68	

D=fractal dimension

C= constant

r/L= ratio of molecule radius to the linear size of fractal system

N= number of layers

V_m= volume of a monolayer

$$s = \sqrt{\frac{\sum_{i=1}^n (y_i - \bar{y})^2}{n-2}}$$

= standard deviation of the volume adsorbed. n is the number of data point ,
 \bar{y} is the modeled volume.

Table 2. Calculated Freundlich Adsorption Isotherm Parameters

	Sorbonorite 4	GAC 1240	Carbon #1	Carbon #3	Carbon #4
k	332	278	0.09	0.08	3.19
1/n	0.77	0.79	0.37	0.35	0.59
R ²	0.92	0.96	0.92	0.89	0.96

* Carbon #2 presented inconclusive results

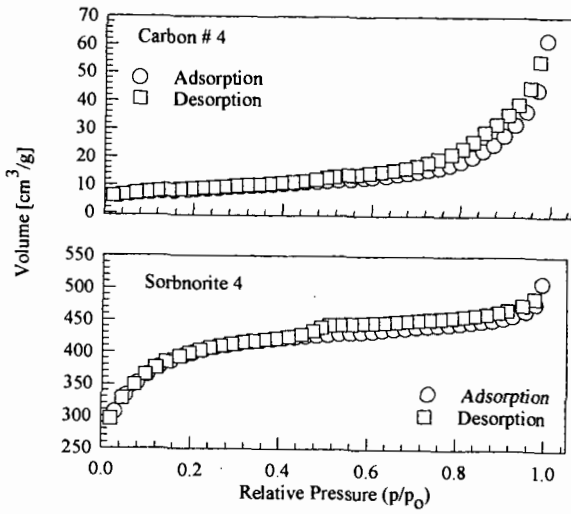


Figure 1. Adsorption and Desorption Isotherms Determined for Carbon #4 and Sorbonorit 4

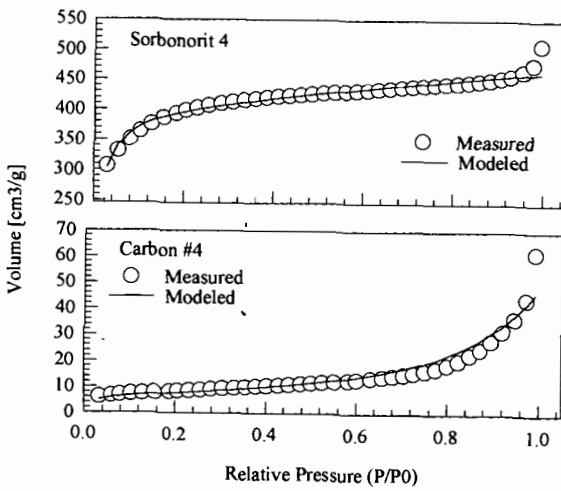


Figure 2. Modeled and Measured Adsorption Isotherms For Sorbonorit 4 and Carbon #4.

HIGH YIELD ACTIVATED CARBON FROM BIOMASS BY AIR ACTIVATION

Xiangfeng Dai and Michael J. Antal, Jr.

Hawaii Natural Energy Institute and the Department of Mechanical Engineering
University of Hawaii at Manoa
Honolulu, HI 96822

INTRODUCTION

With its large internal surface area, activated carbon has extraordinary adsorptive capabilities. It is employed in a wide range of applications, mostly as a purifying agent to remove trace quantities of undesirable species from gas or liquid phase as well as an economical medium to recover precious materials. The demand for activated carbon has been continuously increasing in the past decade. In 1988, the consumption of activated carbon in industrialized countries was 300,000 tons (Roskill, 1990). The United States accounts for 43% of this amount - around 130,000 tons. Since then, the demand in the U.S. market is estimated to have increased at a rate of 5% per year to around 230,000 tons by the year 2000. Because of worldwide increasing environmental problems and stricter regulations set by governments in both industrialized and developing countries, the demand for activated carbon will continue to increase.

Commercial production of activated carbon employs high temperatures of above 800°C using steam or carbon dioxide as an activating agent from coal and limited amount of biomass by thermal activation process. On the other hand, yield of activated carbon from biomass is low, e.g., 5 - 8 % from coconut shell. Consequently, activated carbon produced by conventional method is expensive. The retail price of activated carbon ranges from \$2 - \$6 per kg depending on the type.

In this article, a novel thermal process of producing high-yield activated carbon from Macadamia shells by air or a mixture of air and inert gas at low temperature is discussed. Characteristics of the carbon are presented.

EXPERIMENTAL

Macadamia shells as agricultural by-products in Hawaii are employed as the original material in this work. Raw Macadamia shells are in hemispherical shape with about 25 mm diameter and 3 mm thickness. Macadamia shells undergo a series of pretreatments and post-treatments before forming the final products -- activated carbons. Pretreatments include pyrolysis in a pressurized lab reactor, in which high yield charcoal is obtained as described elsewhere [Dai, 1995; Antal, 1996], and then followed by high temperature carbonization process at atmospheric pressure without oxygen presence. Afterwards, carbonized charcoal is subjected to oxygenation process, in which various operating conditions are investigated to fine tune the final product. The major operating parameters include temperature, total pressure, oxygen partial pressure (P_{O_2}), oxygenation time and carbon burn-off, etc. Finally, oxygenated charcoal receives post-treatment at high temperature, namely, the activation process as termed in this work, degassing or desorption process as termed commonly, thereby forming activated carbon. The raw charcoal retains the shape of its raw shell. The hemispherical charcoal is employed only in the lab reactor. Granulated charcoal particles with 6×14 mesh are employed in both the lab reactor and the ceramic reactor which will be discussed next.

The key step is the oxygenation process. Part of the oxygenation process has been conducted in the lab reactor, with which a detailed arrangement and operating procedure similar to the ceramic reactor is described elsewhere [Dai, 1995]. However, most significant progress was made in the ceramic reactor. The ceramic reactor system is schematically shown in Fig. 1. Pretreated granulated charcoal is loaded in the upper portion of the reactor. Due to strong exothermic reaction in the oxygenation process, nitrogen or helium is mixed with air to serve as a thermal ballast. Air passing a regulator from the air tank is controlled by a micrometering valve and measured using a mass flow controller (Aalorg model GFM-1700) before reaching an on/off valve. Similarly, nitrogen or helium is controlled by a micrometering valve and measured using a rotameter (Brook model 1110-01F1B1A) before passing an on/off valve. Then air and nitrogen/helium are mixed and fed into the 50 mm diameter ceramic reactor. The product gas leaves the reactor to a 3-way valve, one way going to the sampling bag while the other going to a rotary flow meter (GCA/Precision Scientific wet test meter) after a cooling section. The desired temperature is obtained by controlling an external heater with a variable voltage transformer and an internal heater with a temperature controller. A thick bed of glass beads is packed upstream of the charcoal sample layer to improve heat transfer and uniformity of flow. Two type K thermocouples contact the charcoal sample to record the charcoal temperature. Flow meters are calibrated at room temperature before onset of the experiment using a soap film flow meter. Gas samples are taken in the sampling bag as well as in an in-line port with a septum downstream of the 3-way valve. Then, the sample gas is analyzed by a Gas Chromatograph (Hewlett Packard

Model 6890) equipped with a thermal conductivity detector and a column made of two concentric columns capable of separating nitrogen and oxygen (Alltech CTR). The adsorptive properties are reported in terms of iodine number, BET (N_2) surface area, and pore size distribution. Iodine number test follows ASTM D4607-86. BET surface area and pore characteristics are analyzed by a gas sorption analyzer (Quantachrome Autosorb-1).

RESULTS AND DISCUSSION

A series of experiments have been conducted under a range of operating conditions in oxygenation process using nitrogen/air mixture in the lab reactor. A set of typical results is shown in Table 1. As seen in the table, both large and small sized oxygenated charcoal have low iodine number, i.e., 121 mg/g and 282 mg/g, respectively. When surface oxides are removed after post-treatment, iodine number of both activated carbons increases dramatically -- 366 mg/g and 506 mg/g for large and small size. Higher iodine number of small particles is partly due to higher burn-off and probably mostly due to its small size, in which case, the effect of mass transport within charcoal pores is much less important than in large particles. From this result and the fact that granulated or powdered activated carbon is predominantly used in applications, granulated charcoal has been used in this study since then.

Another series of experiments were conducted in the ceramic reactor to reveal conditions for producing high yield, good quality activated carbon. A typical experimental result is shown in Table 2, in which a thick bed of charcoal samples is employed and post-treatment is followed. As seen in the table, yield and iodine number of activated carbon is quite different, depending upon the location in the packed bed. Activated carbon at the bottom layer has a higher iodine number of 652 mg/g with an overall mass yield of 12%, while the top layer has a lower iodine number of 260 mg/g but with a higher mass yield of 29%. This suggests that the overall reaction rate highly depend upon oxygen partial pressure. Activated carbon at the layer next to the bottom seems the best compromise in terms of yield and quality (iodine number). This sample would have an overall yield of around 20% with an iodine number over 700 mg/g if the oxygenation time were longer.

The result of one experiment with a thin layer of carbonized charcoal treated with pure air in the oxygenation process shows that activated carbon with an iodine number of 700 mg/g is obtained, compared to iodine number of 181 mg/g for carbonized charcoal as listed in Table 2. A fraction of this sample burned during oxygenation process as ash was collected from the reactor. Thus, it is crucial to control temperature and oxygen partial pressure in this process. This is one of the reasons why activated carbon is difficult to produce by air/oxygen activation.

The pore size distribution of a typical activated carbon with an iodine number of 625 mg/g is shown in Fig. 2. A double-peaked distribution is observed, one at around 0.8 nm in micropore regime while the other at around 36 nm in mesopore regime. From engineering point of view, this activated carbon has potential to be oxygenated for longer time by creating more pores and/or enlarging micropores so that higher surface area would be obtained. From application point of view, this kind of structure favors fast mass transport of adsorbates with a micropore size into the deep part of the pores compared to uniform micropore dominated pore structure, hence increasing process efficiency.

A TGA analysis on post-treatment of oxygenated charcoal by a colleague (Dr. G. Varhegyi) in Hungarian Academy of Science shows that desorption of surface oxides as CO_2 reaches its peak rate at around 500°C and as CO at around 700°C. Further increase in temperature will shorten the pre- and post-treatment time but may take a risk of having carbon annealed at above 800°C. This confirms our earlier results that a temperature of 750°C is best for pre- and post- treatment of charcoal among temperatures examined at 600°, 750° and 950°C.

CONCLUSION

Activated carbon with a high yield of above 20% from Macadamia shells is realized in a novel process including a series of pre- and post-treatments. This is compared to the 5 - 8% realized by conventional thermal activation method. The key process -- oxygenation is carried out at low temperatures using air or a mixture of air and inert gas as an activating agent. The pore structure and iodine number of 600 - 700 mg/g suggest that this activated carbon have potential of further increasing its surface area by finer tuning of the operating parameters.

ACKNOWLEDGMENTS

This work is supported by the National Science Foundation (Grant # CTS95-21423) and the Coral Industries Endowment of the University of Hawaii. The authors would like to thank Dr. Maria Burka (NSF) for her continuing interest of this work, Dr. Gabor Varhegyi with Hungarian Academy of Science for TGA analysis, Guilherme Bezzon, Dr. Angela Garcia and Dr. Makoto Sakurai for their assistance.

REFERENCES

- Antal, M. J., Croiset, E., Dai, X. et al. "High yield biomass charcoal". *Energy & Fuels*. Vol. 10, No. 3, 652-658, 1996.
- Dai, X., Norburg, N., and Antal, M. J. "Production of charcoal and activated carbon at elevated pressure". *Symposium on Materials and Chemicals Synthesis from Fossil Fuels and Biomass*. ACS, 285-287, 04/95.
- Roskill Information Service, Ltd. "The economics of activated carbon 1900". *PTS Research Studies*. 1-180, 08/90.

Table 1. Results of Macadamia shell activated carbon from the lab reactor

size	burn-off	I.N. (ox) ^a	I.N. (ac) ^b	yield
φ25x3 mm	0.194	121 mg/g	366 mg/g	24%
6x12 mesh	0.667	282 mg/g	506 mg/g	9.4%

^a iodine number of oxygenated charcoal treated at 339°C, P_{O₂}=4.2 kPa in N₂ for 90 min;

^b iodine number of activated carbon.

Table 2. Results of Macadamia shell activated carbon from the ceramic reactor^a

location	yield	iodine number
(carbonized charcoal)	0.30	181
#1 (bottom)	0.12	652
#2	0.25	552
#3	0.27	420
#4	0.28	---
#5 (top)	0.29	260

^a oxygenated at 250°C, P_{O₂}=12.7 kPa in N₂ for 62 min.

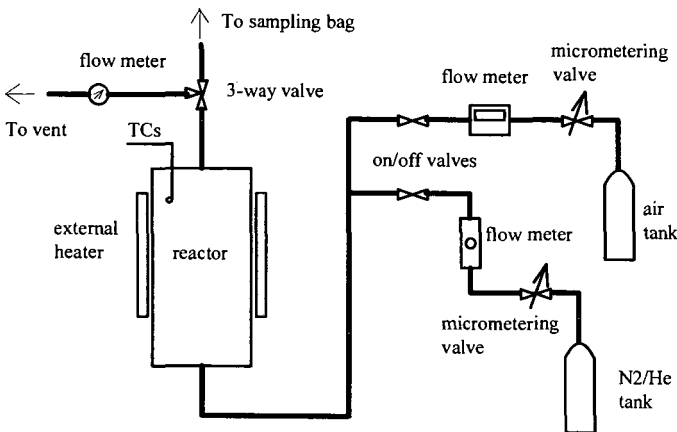


Fig. 1 Schematic of the ceramic reactor for activation

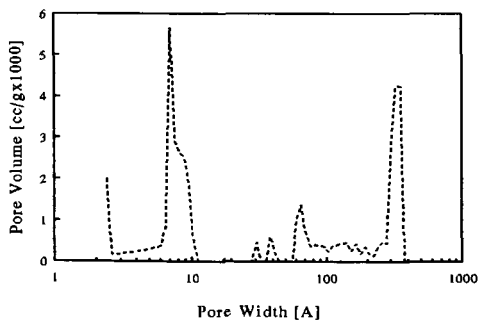


Fig. 2. Pore size distribution of Macadamia shell activated carbon

ACTIVATED CHAR FROM ILLINOIS COAL FOR COMBINED SO₂/NO_x REMOVAL

Anthony A. Lizzio¹, Alex M. Chang² and John L. Haslbeck²

¹Illinois State Geological Survey, 615 East Peabody Drive, Champaign, IL 61820

²NOXSO Corporation, 2414 Lytle Road, Bethel Park, PA, 15102

Keywords: activated char, sulfur dioxide, nitrogen oxides.

INTRODUCTION

Carbon-based processes for flue gas cleanup operating in Europe [1] and Japan [2] today typically use two reactors, one to remove SO₂ and the other to remove NO_x with ammonia injection. One of the major impediments to the commercialization of this technology in the U.S. has been the cost of the activated carbon used and the fact that there is no commercial carbon on the market today that can simultaneously remove both SO₂ and NO_x from coal combustion flue gas. The NOXSO Corporation has developed a dry, post-combustion flue gas treatment system that uses a regenerable sorbent (alumina beads impregnated with 5% sodium) in a fluidized bed for combined SO₂/NO_x removal [3]. The IGS and NOXSO are working together to develop a low cost sorbent from bituminous coal to use as an alternative sorbent in this process [4].

Numerous studies have examined NO_x removal by carbon at 300-600°C, although it is most convenient and economical to remove NO_x from flue gas at lower temperatures (100-150°C). Some studies have not used O₂ in the simulated flue gas when testing their carbons, and nearly all studies have neglected the effect of H₂O on NO_x removal. Whether activated carbon can remove significant amounts of NO_x in the presence of both H₂O and SO₂, i.e., without having to inject ammonia into the flue gas, remains to be determined. With such a carbon, only one reactor would be required to remove both SO₂ and NO_x from coal combustion flue gas. Today, two reactors are used because ammonia tends to react with sulfur dioxide and carbon to form ammonium sulfate, which is detrimental to activated carbon performance.

The overall objective of this study [4, 5] has been to develop a low cost activated char from bituminous coal for simultaneous removal of SO₂ and NO_x from coal combustion flue gas. Such a carbon could be used in the NOXSO process as well as in traditional fixed-bed and (less capital intensive) carbon injection processes. In this paper, we begin by examining the effect of H₂O and SO₂ on NO_x removal by activated chars shown previously in our laboratory to work well in removing SO₂ from simulated flue gas [6]. We also develop new carbons and explore the possibility of adding a catalyst to or ammonia treating activated char to enhance its combined SO₂/NO_x removal capabilities.

EXPERIMENTAL

Activated chars were prepared from an Illinois hvC bituminous coal (IBC-102) [7]. Figure 1 shows the various processing steps that were used. A 2 in. ID batch, fluidized-bed reactor (FBR) was used to pyrolyze 200 g of 48x100 mesh coal (N₂, 900°C, 0.5 h) and activate the resultant char (H₂O, 860°C, 30% conversion). The steam activated char was treated with nitric acid (10 M HNO₃, 80°C, 2 h) and thermally desorbed in N₂ or H₂ at 925°C for 1 h to desorb carbon-oxygen (C-O) complexes. A KOH activated char was prepared by mixing KOH with IBC-102 coal (2:1 KOH/coal) and pyrolyzing in the FBR (N₂, 800°C, 1 h). To prepare catalyzed chars, potassium (acetate) or sodium (carbonate) was added to IBC-102 coal by incipient wetness (IW) and pyrolyzed in N₂ (750°C, 0.5 h); the resultant char was activated in CO₂ (720°C, 2 h). In addition, K or Na was ion-exchanged (IE) onto HNO₃ treated char. Selected chars were also treated with anhydrous NH₃ at 900°C for 2 h.

A fixed-bed adsorber (1 cm ID x 30 cm stainless steel tube) connected to a quadrupole mass spectrometer (VG Quadrupoles, Fisons Instruments) was used to obtain SO₂ and NO breakthrough curves. Typically, 6 g of char (8 cm bed height) was placed between two layers of quartz wool and heated to 120°C in flowing He (0.2 L/min). The He flow was switched to 2500 ppm SO₂, 500 ppm NO, 5% O₂ and 7% H₂O, balance He (space velocity = 2000 h⁻¹). The char sample was regenerated in situ by heating it in flowing N₂ to 525-925°C.

RESULTS AND DISCUSSION

Figure 2 presents NO breakthrough curves for several IBC-102 chars and a commercial activated carbon, Centaur carbon (Calgon Carbon). Centaur (B) removed little NO_x at 120°C, whereas the thermally desorbed IBC-102 chars (C-G) performed significantly better. The air oxidized/thermally desorbed IBC-102 char (D) was slightly better than the KOH activated char (A). Exposure of the char sample to ambient air for 48 h prior to a NO_x removal run had a detrimental effect on performance (compare C and E). Chemisorbed oxygen may poison active sites for NO adsorption/reduction. The absence of adsorbed oxygen enhances SO₂ removal by carbon [8, 9]. Carbon atoms not occupied by adsorbed oxygen atom have valence electrons more available and reactive towards SO₂. These unoccupied or free sites control adsorption of SO₂ [9] and perhaps NO_x. Figure 2 also shows that Sample G (sample E heated to 925°C in H₂ instead of N₂) removed nearly twice as much NO_x as sample E. Treatment of char with H₂ at this temperature serves to gasify the most reactive carbons leaving behind a more stable surface, but one that still contains free sites. The more stable surface adsorbs less O₂ and H₂O at room temperature, which leads to more available sites for reaction with NO_x at 120°C.

Recent results in the literature seem to suggest that low temperature NO_x removal by activated carbon in the presence of SO₂ is not possible [10]. Figure 3 shows the effect of SO₂ and H₂O on NO_x removal by the IBC-102, HNO₃, 925°C char. The char removes 98% of the NO_x for about 1.5 h, then NO partially breaks through to about 200 ppm. For the next 15 h the [NO] increases from 200 to 300 ppm. Two NO_x removal mechanisms seem to be in effect. One where NO is simply adsorbed on the char surface and the other where the char converts NO to N₂. The catalytic mechanism

could account for incomplete breakthrough. When both SO_2 and H_2O are added at $t = 17$ h, large amounts of NO are desorbed. Figure 3 shows that SO_2 or H_2O (or both) displace adsorbed NO_x . This char also adsorbed the expected amount of SO_2 (111 mg SO_2/g char) even though the char was saturated with NO_x . Note that when SO_2 and H_2O were added, NO_2 was also desorbed from the char. The NO_2 desorption peak appears to coincide with the NO peak. Figure 4 shows the effect of adding H_2O and SO_2 at different times during NO_x removal. Note that the catalytic component of the breakthrough curve (200-500 ppm) no longer persists after H_2O is added. The SO_2 capacities of the IBC-102, HNO_3 , 925°C chars in Figures 3 and 4 were quite similar, 111 and 99 mg SO_2/g char, respectively.

Effect of Potassium

Figure 5 shows NO breakthrough curves for char prepared from IBC-102 coal loaded with 6% K by IW. This char has a N_2 BET surface area of only 100 m^2/g compared to 500-600 m^2/g for the uncatalyzed chars shown in Figures 3 and 4. The NO breakthrough curve (no H_2O) fails to exhibit a initial period of 95-100% NO_x removal. Thermal desorption at 925°C, however, results in a 2 h period of > 98% NO removal. Thermal desorption creates free sites for NO adsorption. Figure 5 shows that this char also removes > 98% NO for about 1 h after 7% H_2O is added. A Na-loaded char prepared in a similar fashion also adsorbed NO_x with H_2O , but not to this extent.

The data shown in Figure 5 were promising. The surface area of this char could be increased through further activation, and the surface chemistry or in this case, catalyst dispersion, could be enhanced by using ion exchange instead of impregnation to load K onto the char. In an attempt to do this, steam activated IBC-102 char was treated with nitric acid, then placed in a solution of 1 M potassium acetate. The ion-exchanged char (IBC-102, HNO_3 , K, IE) was then thermally desorbed at 925°C to remove chemisorbed oxygen and fix potassium atoms on the carbon surface. Figure 6 presents NO breakthrough curves with and without H_2O and SO_2 for an activated char prepared in this way (IBC-102, HNO_3 , K, IE, thermally desorbed at 525°C and/or 725°C). Sample A (525°C) removed > 98% of the NO for more than 12 h without H_2O in the simulated flue gas. With H_2O and SO_2 added at $t = 0$ h, this char (B) performed very well in removing 98% of the NO_x for 2 h. Regeneration at 725°C (C) reduced its effectiveness, perhaps because K volatilizes at $T > 700^\circ\text{C}$. When H_2O and SO_2 were again removed from the gas stream (D), NO_x removal performance improved, but not to previous levels (A).

Recent studies [11-13] have shown that K is a good catalyst for NO_x removal (without H_2O or SO_2) at relatively high temperatures (300-600°C). In TPR experiments (5°C/min), K-loaded char appeared to remove some NO , beginning at 100°C, but it was not clear how much or whether it was even a significant amount [13]. To the best of our knowledge, the results obtained with IBC-102, HNO_3 , K, IE char show for the first time that significant amounts of NO_x can be removed by activated char at 120°C in the presence of H_2O and SO_2 .

Effect of Ammonia Treatment

Figure 7 shows NO breakthrough curves for steam activated IBC-102 char and the same char treated with ammonia at 900°C for 2 h. These runs, performed without H_2O in the flue gas, show that the NH_3 treatment increases the NO_x breakthrough time from 0 h to about 3 h. The ammonia treatment incorporates nitrogen into the char structure as NH_3 , dissociates into N and H_2 at elevated temperatures. The H_2 can gasify the carbon if the temperature is high enough, and also deposit on the carbon surface to preserve the free sites for NO_x removal as shown in Figure 2. The surface area of the steam activated IBC-102 char increased from 465 to 580 m^2/g after the 2 h ammonia treatment. The incorporated nitrogen can have special catalytic properties. Stohr et al. [14] discussed how treatment of carbon with ammonia or hydrogen cyanide at elevated temperatures resulted in a dramatic increase in catalytic activity in oxidation reactions. The catalytic nitrogen was hypothesized to be surrounded by three carbon atoms and was situated near or at the edge of the basal plane. Most recently, Fei et al. [15] postulated that the relatively high nitrogen content of activated carbon fibers derived from shale oil was responsible for their enhanced SO_2 removal capabilities at room temperature compared to a commercial activated carbon fiber made from coal tar pitch. In our case, the NH_3 treatment has apparently increased the catalytic activity of steam activated IBC-102 char for reduction of NO to N_2 and O_2 . Without the NH_3 treatment, the steam activated IBC-102 char has no activity for NO_x reduction (Figure 7).

Figure 8 shows the effect of H_2O on NO_x removal by the NH_3 treated, H_2O activated IBC-102 char. Water in the flue gas inhibits NO_x removal by IBC-102 char, but it is important to note that even in the presence of H_2O , the NH_3 treated char removes 90% of the NO_x for about 1 h, which means that the catalytic properties of incorporated nitrogen are retained even in the presence of H_2O . Figure 9 shows the effect of thermal desorbing the NH_3 treated, H_2O activated IBC-102 char at 925°C for 1 h prior to a NO_x removal experiment (with no H_2O in the flue gas). There is no appreciable difference in these two NO breakthrough curves indicating that the NH_3 treatment at 900°C for 2 h essentially acts as a thermal desorption treatment in N_2 at 925°C for 1 h with respect to its effect on free site concentration.

Figure 10 shows NO breakthrough curves for the NH_3 treated, H_2O activated char and the NH_3 treated, HNO_3 treated, H_2O activated char. HNO_3 treatment of the char following H_2O activation, but prior to NH_3 treatment, increases the breakthrough time from about 4 h to 10 h (without H_2O in the flue gas), a significant improvement in NO_x removal performance. Ammonia will tend to react more vigorously with the free sites generated by the nitric acid treatment than with those of the steam activated char. Nitric acid treatment of steam activated char and subsequent desorption of carbon-oxygen complexes has been shown to increase the number of carbon free sites for SO_2 adsorption [6, 9]. The generation of free sites also seems to enhance NO_x removal by activated char. Figures 3 and 4 show that SO_2 and NO_x compete for similar adsorption sites since NO_x is desorbed from the char when SO_2 is first introduced into the flue gas. Figure 10 also shows the effect of H_2O in the flue gas on NO_x removal by the NH_3 treated, HNO_3 treated, H_2O activated IBC-102 char. The NO breakthrough time is reduced by about one half, but this char still shows considerable catalytic activity. The combination of free sites and incorporated nitrogen atoms generated from the HNO_3 and NH_3 ammonia treatments, respectively, has resulted in the best performing char to date, i.e., greater than 90% NO_x removal for 4 h in

the presence of H₂O. This performance is twice as good as our previous best char (see sample B, the ion exchanged K loaded IBC-102 char, in Figure 5). A way to lower the cost of making this char would be to air oxidize (instead of HNO₃) the H₂O activated char and then react it with ammonia. The goal would be to achieve comparable SO₂/NO_x removal performance with air oxidation as was achieved with the HNO₃ treatment. The ion exchange of potassium onto this char under pH controlled conditions (pH = 9-11) could further enhance its combined SO₂/NO_x removal capabilities.

Figure 11 presents SO₂ adsorption profiles for the Centaur carbon; H₂O activated IBC-102 char; HNO₃ treated, H₂O activated char; and KOH activated char, and for these same chars treated with NH₃ at 900°C for 2 h. Three of the six IBC-102 chars outperform the commercial carbon. Ammonia treatment increases by up to 50% the SO₂ capacity (at 6 h) of these chars, which is quite remarkable. We postulate that the incorporation of nitrogen into the char and possibly the deposition of hydrogen on the char surface contributes to this dramatic increase in SO₂ adsorption capacity. The N₂ BET surface areas of the H₂O activated char and HNO₃ treated, H₂O activated char increased from 465 and 827 m²/g to 580 and 860 m²/g, respectively. The surface area of the NH₃ treated, KOH activated char remained unchanged at 1100 m²/g. The NH₃ treated, HNO₃ treated, H₂O activated char had the highest SO₂ capacity (520 mg SO₂/g at 6 h) of any Illinois coal char or commercial activated carbon tested to date. This char performed well in removing NO_x in the presence of H₂O and shows tremendous potential in removing SO₂ from simulated flue gas. It is the leading candidate for use in the NOXSO process.

Integration of Activated Char into NOXSO Process

Several options are being considered for integrating ISGS activated char into the NOXSO process. One process configuration involves using activated char in a two stage system, each stage being a fluidized- or fixed-bed adsorber. The first bed could contain activated char (e.g., H₂O activated IBC-102 char) that removes greater than 98% of the SO₂ from the flue gas, but little NO_x. The second bed could contain activated char (e.g., H₂O activated, HNO₃ or air oxidized, K-catalyzed IBC-102 char) that removes greater than 90% of the NO_x from essentially SO₂-free flue gas that contains 5-12% H₂O. This char could achieve relatively high NO_x removal rates without the use of additional reagents such as ammonia. Another and probably the best scenario is to use one char and one reactor to remove both SO₂ and NO_x from the flue gas. This char could be the NH₃ treated, oxidized (either by air or nitric acid) IBC-102 char shown to remove large amounts of NO_x and SO₂ from simulated flue gas (Figures 10 and 11). Another place to use activated char in the NOXSO process would be in the reheater recycle stream. If NO_x could be removed at this point in the process it would increase the overall operating efficiency of the power plant that uses the NOXSO process to clean flue gas. Instead of sending NO_x laden flue gas back to the boiler where excess NO_x is converted to N₂, a bed of activated char could be used to remove NO_x from this waste stream. The power plant could then operate independently of the NOXSO process, which is more favorable. Based on the results obtained in this study, addition of activated char to these locations in the NOXSO process (in or downstream of the fluidized-bed adsorber and/or in the reheater recycle stream) could improve the overall efficiency and lower operating costs of the NOXSO process.

CONCLUSIONS

Activated chars were prepared from Illinois coal and combined SO₂/NO_x removal experiments performed to examine the competitive effects of H₂O and SO₂ on low temperature NO_x removal. The SO₂ capacity of the char was not affected to any appreciable extent by NO in the flue gas. Both H₂O and SO₂ appeared to inhibit NO adsorption by activated char. One ion exchanged K-catalyzed char showed exceptional promise since it adsorbed significant amounts of NO even with H₂O in the gas stream. Nitric acid and/or ammonia treatment of steam activated IBC-102 char also enhanced its NO_x removal capabilities. The combination of free sites and incorporated nitrogen atoms generated from the HNO₃ and NH₃ ammonia treatments, respectively, resulted in a char that removed greater than 90% NO_x removal for 4 h in the presence of H₂O. Moreover, the NH₃ treatment of IBC-102 char increased its SO₂ adsorption capacity by up to 50%. The NOXSO process could incorporate activated char in one or more locations in their process or it may be that an entirely new process is designed based on the unique SO₂/NO_x removal capabilities of activated char.

ACKNOWLEDGEMENTS

This work was supported by the Illinois Clean Coal Institute through the Illinois Coal Development Board and the United States Department of Energy. The authors gratefully acknowledge the technical assistance of Gwen Murphy, Gwen Donnals and Sheila Desai.

REFERENCES

1. Hartenstein, H.-U., *ACS Preprints, Div. Fuel Chem.* 41 (1), 409 (1996).
2. Tsuji, K. and Shiraishi, *JCS Preprints, Div. Fuel Chem.* 41 (1), 404 (1996).
3. Ma, W.T. and Haslbeck, J.L., *Environmental Progress* 12, 163 (1993).
4. Lizzio, A.A., Cal, M.P., DeBarr, J.A., Donnals, G.L., Haslbeck, J.L., Chang, A.M. and Banerjee, D.D., "Development of Activated Char for Combined SO₂/NO_x Removal," Final Technical Report to Illinois Clean Coal Institute, 1996.
5. Lizzio, A.A., DeBarr, J.A. and Kruse, C.A., *Energy and Fuels* 11, 250 (1997).
6. Lizzio, A.A. and DeBarr, J.A., *Fuel* 75, 1515 (1996).
7. Demir, I., Lizzio, A.A., Fuller, E.L. and Harvey, R.D., *J. Coal Quality* 13, 93 (1994).
8. Mochida, I., *Energy and Fuels* 11, 272 (1997).
9. Lizzio, A.A. and DeBarr, J.A., *Energy and Fuels* 11, 284 (1997).
10. Jang, B.W.-L., Spivey, J.J., Kung, M.C. and Kung, H.H., *Energy and Fuels* 11, 299 (1997).
11. Illan-Gomez, M.J.; Linares-Solano, A.; Salinas-Martinez de Lecea, C. and Calo, J.M., *Energy and Fuels* 9, 97 (1993).
12. Illan-Gomez, M.J.; Linares-Solano, A.; Radovic, L.R., Salinas-Martinez de Lecea, C. *Energy and Fuels* 9, 104 (1995).
13. Garcia-Garcia, A., Linares-Solano, A., Salinas-Martinez de Lecea, C., *Energy and Fuels* 11, 292 (1997).
14. Stohr, B., Boehm, H.P. and Schlogl, R., *Carbon* 29, 707 (1991).
15. Fei, Y., Sun, Y., Givens, E. and Derbyshire, F., *ACS Preprints, Div. Fuel Chem.* 40 (4), 1051 (1995).

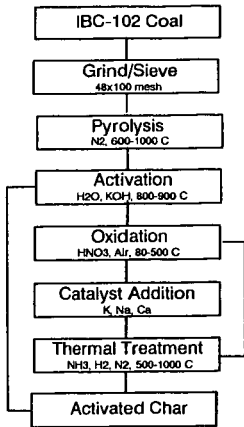


Figure 1. Production of activated char from Illinois coal.

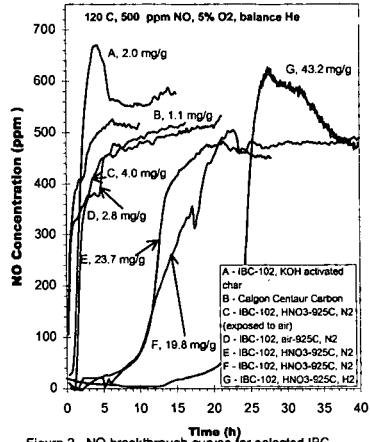


Figure 2. NO breakthrough curves for selected IBC-102 chars and a commercial activated carbon.

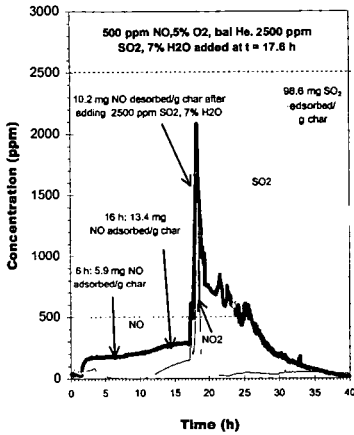


Figure 3. Effect of adding SO₂ and H₂O at the same time on NO_x removal by IBC-102, HNO₃, 925 C char.

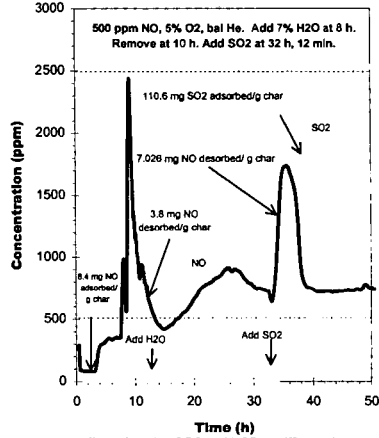


Figure 4. Effect of adding SO₂ and H₂O at different times in NO_x removal by IBC-102, HNO₃, 925 C char.

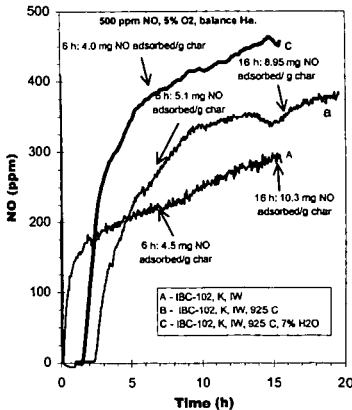


Figure 5. Effect of thermal desorption treatment (925 C) and H₂O on NO_x removal by IBC-102, K, IW char.

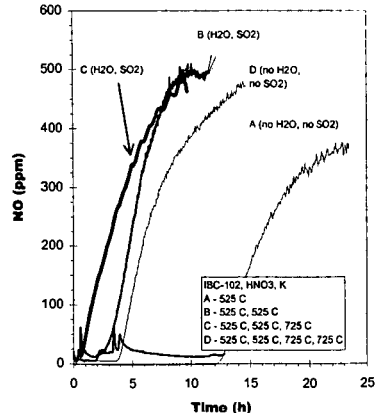


Figure 6. Effect of thermal desorption temperature and H₂O/SO₂ on NO_x removal by IBC-102, HNO₃, K, IE char.

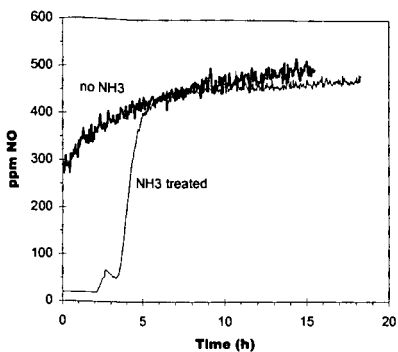


Figure 7. Effect of NH₃ treatment on NO_x removal by steam activated IBC-102 char.

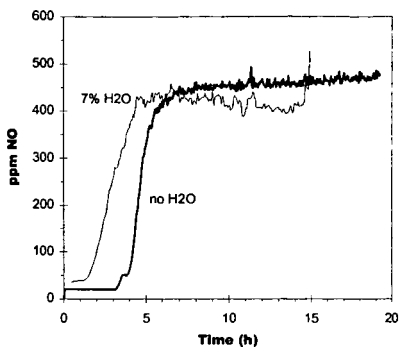


Figure 8. Effect of H₂O on NO_x removal by NH₃ treated, steam activated IBC-102 char.

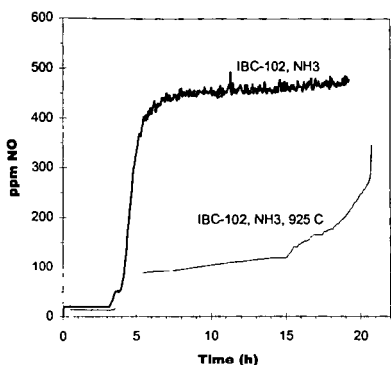


Figure 9. Effect of thermal desorption treatment at 925 C on NO_x removal by NH₃ treated, steam activated IBC-102 char.

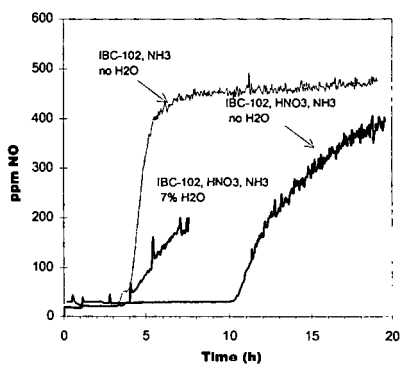


Figure 10. Effect of HNO₃ treatment on NO_x removal by NH₃ treated, steam activated IBC-102 char.

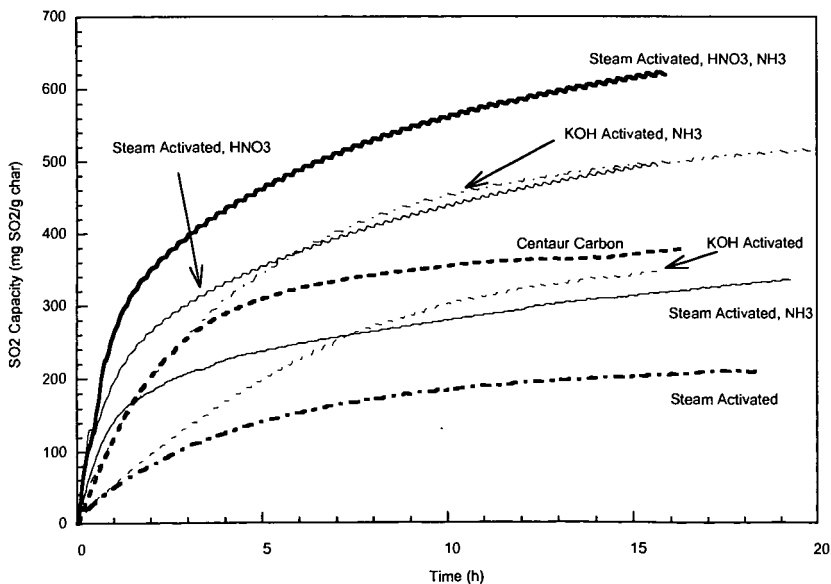


Figure 11. Effect of NH₃ treatment on SO₂ adsorption capacity of selected IBC-102 chars.

CLEANUP OF HOT COAL GAS WITH CARBON-BASED SORBENTS

Mark P. Cal^{1,2}, Brooks W. Strickler^{1,2}, Anthony A. Lizzio¹, Mark J. Rood²

¹Illinois State Geological Survey, 615 E. Peabody Dr./MC-650, Champaign, IL 61820

²University of Illinois, Department of Civil and Environmental Engineering/MC-250, Urbana, IL

Keywords: gasification, adsorption, hydrogen sulfide.

INTRODUCTION

Integrated Gasification Combined Cycle (IGCC) power systems are emerging as the most promising technology to convert high sulfur coal into electricity. Illinois Basin coal is a proven feedstock for IGCC, e.g., the Destec process in Terre Haute, IN. Hot gas cleanup for desulfurization is needed to accelerate the successful demonstration and commercialization of advanced coal gasification systems worldwide. In IGCC processes, hydrogen sulfide is removed from the coal gas before it enters the turbine. To achieve maximum efficiency in IGCC systems, H₂S should be removed from the fuel gas while hot. Although H₂S can be removed quite effectively by cooling the hot gases to temperatures less than 100°C, removal of H₂S at 300-800°C can lead to significant increases (up to 3%) in overall thermal efficiency. More efficient IGCC processes expand for markets hot gas cleanup sorbents and for high sulfur Illinois coal.

Numerous metals and mixed metal compounds have been studied as possible desulfurization sorbents. Current leading sorbents include zinc titanate and Z-Sorb (a proprietary zinc-oxide-based sorbent). However, not only are these sorbents expensive (up to \$7-15/lb), they are also prone to chemical and/or physical degradation during cycling. Zinc titanate suffers from spalling due to formation of sulfide and sulfate which have 2 to 3 times higher molar volume than the oxide. Z-Sorb degrades in the presence of steam present in coal gas. Both sorbents sinter during regeneration and typically their reactivity drops by around 50 percent in just 50 cycles.

One may conclude by reviewing the literature on hot gas cleanup sorbents that while research on sorbent materials has been extensive, continuing efforts are important because these sorbents are not yet used commercially in coal gasification processes, and there is still time for the development of improved sorbents. Another reason to encourage research in this area is that not all gasification systems are alike, and because of these differences in operating conditions and requirements, it is likely that more than one type of sorbent will be needed to satisfy the market. Every sorbent examined to date has had at least one major deficiency that prevents its widespread use. The fact that there is still ample opportunity to develop new types of sorbents for hot gas cleanup provides incentive for research on new types of materials.

One material that should be examined in more detail as a potential hot gas cleanup sorbent is carbon. Although, the use of carbon for hot gas cleanup has significant potential, the possibility of using carbon-based materials to remove sulfur containing gases from the products of coal gasification has been overlooked as other sorbents such as zinc ferrite, zinc titanate, and copper oxides have been extensively studied. Carbon has several advantages compared to metal-based hot gas cleanup sorbents: 1) the harsh coal gas environment should not affect the properties of the carbon during operation (carbon will not gasify in a reducing atmosphere at temperatures less than 700°C), 2) carbon, itself, adsorbs large quantities of H₂S, meaning that it could be used as an active support for metals such as copper and zinc which also adsorb H₂S; most metal-based sorbents have an inert support matrix, sometimes constituting up to 60% of the mass of the sorbent, 3) carbon will not chemically spall unlike metal based sorbents and it is more physically stable, since there is little or no volumetric change in a carbon-based sorbent due to sulfur loading, and 4) coal, which is used to make the carbon-based sorbents, is a very inexpensive starting material.

EXPERIMENTAL PROCEDURES

Sorbent Preparation

Activated chars were produced from size-graded Illinois coal in a fluidized-bed reactor (2 in. ID) under controlled preoxidation, pyrolysis, and activation conditions. Preoxidation of the chars was typically performed for 2 hr at 225°C, pyrolysis for 1 hr at 425°C and activation in steam for 2-6 hr at 825°C. Coal samples were activated until a specified carbon conversion was achieved (10-50%). Chars were oxidized using nitric acid (45 wt. % HNO₃) to achieve oxygen concentrations on the chars of up to 15 wt. %. An thermal desorption treatment (200-1000°C) was used to prepare chars with varying amounts of oxygen, which served as a starting material for the metal impregnation step. Various metals (Zn, Cu, etc.) known to chemically react with H₂S were added to the activated char using either incipient wetness or ion exchange methods.

Fixed-Bed Breakthrough Experiments

H₂S removal tests were performed on the various carbon-based sorbents produced in this study. A simulated coal gas stream was used containing 0-50% CO₂, 49-99.5% N₂, and 0.5-1% H₂S at 1 atm and 400-550°C. Initial H₂S adsorption experiments were performed using a 1 cm I.D. 316L stainless steel reactor, but since H₂S reacts with stainless steel at the temperatures examined, only total sulfur measurements are reported for those experiments and not breakthrough times. The measurement technique used to determine the total sulfur added to the carbon is discussed below.

A quartz reactor with a 1.5 cm O.D. and a fritted quartz plate was used for the sulfidation breakthrough tests. The fittings and tubing entering and exiting the reactor are made of teflon in order to minimize the adsorption of H₂S onto anything other than the sorbent being tested. Breakthrough curves were developed at space velocities of about 2000 hr⁻¹ (200 cm³/min) for packed-beds containing the carbon-based sorbents. H₂S influent and effluent concentrations were measured with a mass spectrometer (MS). For most experiments, breakthrough curves were run until the effluent concentration reached 200-300 ppmv. At which time, the experiment was terminated and the breakthrough curve was integrated to yield the total H₂S capacity and the time to breakthrough. Total sulfur analysis was performed on valid samples as a quality assurance/quality control (QA/QC) procedure.

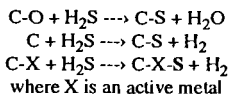
Total Sulfur Measurements

After adsorption and regeneration experiments, total adsorbed sulfur was determined by elemental analysis of the char using a solid state infrared detector (LECO SC-32). Samples were combusted in an oxygen atmosphere where the sulfur oxidizes to SO₂ and were then measured by a solid state infrared detector. The measured SO₂ was then converted to total percentage of sulfur. The sulfur content of samples before and after H₂S adsorption experiments was measured in order to calculate the total sulfur adsorbed.

RESULTS AND DISCUSSION

The best carbon-based sorbents developed for H₂S removal to date had a breakthrough time to 200 ppmv outlet H₂S concentration of over six hours and sulfidation capacities of up to 13 wt. % were observed. Numerous adsorption experiments were performed to evaluate the adsorption capacities and breakthrough times of various carbon-based sorbents. Activated, nitric acid oxidized, desorbed (with more active carbon sites), and metal impregnated chars were used for adsorption experiments. Experimental conditions were altered for a few adsorption experiments to determine their effect on H₂S adsorption. The inlet gas stream was modified to include only H₂S and N₂ in two experiments (Char F & G) and the reactor temperature was lowered from 550 to 400°C for one experiment (Char I). The characteristics and total added sulfur (initial sulfur in the sorbents was about 1 wt. %) for adsorption experiments run with the stainless steel reactor are shown in Table 1. The sulfur content of the chars before and after H₂S adsorption was measured.

A comparison of the sulfur contents of different chars produced several interesting results. As displayed in Table 1, char E had the highest sulfur content after adsorption experiments. Char E was oxidized with nitric acid and impregnated by ion exchange with zinc. The nitric acid oxidized chars (A and B) adsorbed 10.2 to 11.3 wt. % sulfur. A char desorbed of oxygen (char C) adsorbed a significant amount of sulfur (6.5 wt. %), but did not perform as well as the oxidized or metal impregnated chars. This suggests that while carbon sites will adsorb H₂S, oxygen and metal content are also important to achieve optimal adsorption. Char B and C differ in oxygen content only. The oxidized char (B) adsorbed about 50% more sulfur than the desorbed char (C) for comparable adsorption times. It may be concluded from Table 1 that the presence of chemisorbed oxygen enhances H₂S adsorption on activated char. Based upon our measurements to date, we propose three possible routes for H₂S adsorption on carbon:



The total sulfur results in Table 1 suggest the importance of the inlet gas stream. The inlet gas was modified to include only H₂S and N₂ for adsorption experiments with chars F and G. Without CO₂ present in the influent gas stream, the measured adsorption capacities were significantly lower with CO₂. This occurrence can be seen when chars F and G are compared to A and J, respectively. Char A adsorbed about 50% more sulfur than char F for comparable adsorption times and char J adsorbed about 50% more sulfur than char G for a shorter adsorption time. The only difference between these experiments was the presence of CO₂. This occurrence suggests

some interaction between the carbon surface and CO_2 , but it is known that carbon should not gasify in a reducing environment below 700°C . The importance of CO_2 in H_2S adsorption continues to be studied and more research is necessary before any type of conclusion can be suggested.

The total sulfur results in Table 1 indicate the importance of char surface area and reactor temperature. By comparing the surface areas of metal impregnated chars (E, H, N, and O), it can be seen that incipient wetness (IW) reduces surface area to a greater extent than ion exchange (IE). The reduced surface area appears to slightly lower adsorption capacity for similar chars (H and O). The influence of reactor temperature can be seen by comparing chars I and J in Table 1. Char J (550°C) adsorbed significantly more sulfur than char I (400°C) during a shorter run time.

Table 1 also displays total sulfur content of chars after adsorption experiments with the quartz reactor. Chars impregnated with metals (N and O) adsorbed about 10.5 wt. % sulfur before the effluent H_2S concentration reached 500 ppmv (350-390 min). An oxidized char (K) that was run for a longer time (610 min) attained a added sulfur content of 12.7 wt. %. A steam activated char (M), with no nitric acid oxidation, achieved a added sulfur content of 6.1 wt. %. The results show that significant amounts of sulfur (6.1-10.6 wt. %) can be added to carbon in fairly short adsorption times (<400 min). The sulfur contents for chars K-O (quartz reactor) are comparable and slightly better than those of chars A-J (stainless steel reactor). The improvements in adsorption capacities and breakthrough times are most likely due to improved char preparation methods.

Figure 1 displays breakthrough curves for four adsorption experiments with the quartz reactor. Breakthrough times to 200 ppmv outlet H_2S concentration for chars K, M, N, and O ranged from 4-6.5 hours. These breakthrough times were performed at 550°C , a space velocity (SV) of $1700\text{-}2000\text{ hr}^{-1}$ ($200\text{ cm}^3/\text{min}$), and an influent concentration of 5000 ppmv H_2S . The oxidized char impregnated with zinc by ion exchange performed the best, followed by the copper impregnated char. The oxidized char (K) displayed a leveling off of outlet concentration at 1300-1500 ppmv H_2S which is similar to previous adsorption experiments. This may indicate that a catalytic reaction might be occurring which converts H_2S to another compound or it may mean that H_2S adsorption on carbon exhibits a two-stage breakthrough curve. An interesting discovery of the adsorption experiments was that the steam activated char (M) had a breakthrough time (200 ppmv) that was very similar to that of the oxidized char (K).

SUMMARY AND CONCLUSIONS

Results of this project to date have shown that carbon-based sorbents are still adsorbing H_2S at sulfur loadings of 6 to 13 wt. % sulfur from a gas stream containing 0.5% hydrogen sulfide (H_2S) in CO_2 and N_2 at 550°C . Fixed-bed breakthrough curves have been obtained for several chars using a simulated coal gas stream containing 0.5% H_2S at a space velocity of 2000 hr^{-1} ($200\text{ cm}^3/\text{min}$). Breakthrough times to 200 ppmv effluent H_2S concentration ranged from 2 to 6.5 hours, depending on the char used. These breakthrough times are comparable to some metal-based sorbents. Results of adsorption properties are encouraging and show that carbon may be a viable hot gas cleanup sorbent. With further research, we believe that we can increase both the sulfidation capacity and breakthrough time of carbon-based sorbents. It remains to be determined how the pore structure and surface chemistry of the char can be modified to maximize H_2S adsorption capacity. The mechanism of H_2S removal by carbon is also not well understood, and any research to optimize the H_2S removal capabilities of carbon will inevitably lead to new insights into H_2S adsorption and conversion to elemental sulfur on the carbon surface. One distinct advantage carbon has over metal-based is that carbon, itself, adsorbs large quantities of H_2S , meaning that it could be used as an active support for metals such as copper and zinc which also adsorb H_2S . Most metal-based sorbents have an inert support matrix, sometimes constituting up to 60% of the mass of the sorbent. Metal-based sorbents, such as zinc titanate and Phillips Z-Sorb have an inert support matrix that does not participate in the H_2S adsorption reaction.

ACKNOWLEDGEMENTS

This work was supported by the Illinois Department of Energy and Natural Resources through the Illinois Coal Development Board and the Illinois Clean Coal Institute. Discussions with John Lytle and Deepak Tandon of the Illinois State Geological Survey and Santosh Gangwal of the Research Triangle Institute are also appreciated.

Table 1: Carbon-Based Sorbents Analyzed for H₂S Adsorption.

Sorbent ID	Inlet Gas Composition	Oxygen on Sorbent [wt %]	BET Surface Area [m ² /g]	Char Description	Sulfur Added [wt %]	Adsorption Time [min]
Stainless Steel Reactor						
A	0.5% H ₂ S, 49.5% N ₂ , 50% CO ₂	12-15	567	HNO ₃ oxidized	10.2	750
B	0.5% H ₂ S, 49.5% N ₂ , 50% CO ₂	12-15	567	HNO ₃ oxidized	11.3	1200
C	0.5% H ₂ S, 49.5% N ₂ , 50% CO ₂	~0	-	desorbed of oxygen	7.55	1350
D	0.5% H ₂ S, 49.5% N ₂ , 50% CO ₂	12-15	465	HNO ₃ oxidized	11.6	1100
E	0.5% H ₂ S, 49.5% N ₂ , 50% CO ₂	12-15	509	HNO ₃ oxidized + Zn by IE	13.2	1100
F	0.5% H ₂ S, 49.5% N ₂ , 50% CO ₂	12-15	465	HNO ₃ oxidized	6.54	830
G	0.5% H ₂ S, 99.5% N ₂	~0	-	desorbed of oxygen	3.12	460
H	0.5% H ₂ S, 49.5% N ₂ , 50% CO ₂	12-15	130	HNO ₃ oxidized + Cu by IW	10.0	1060
I	0.5% H ₂ S, 49.5% N ₂ , 50% CO ₂	12-15	465	HNO ₃ oxidized, 400°C	2.41	410
J	0.5% H ₂ S, 49.5% N ₂ , 50% CO ₂	12-15	465	HNO ₃ oxidized	4.78	180
Quartz Reactor						
K	0.5% H ₂ S, 49.5% N ₂ , 50% CO ₂	10-15	567	HNO ₃ oxidized	12.7	610
L	0.5% H ₂ S, 49.5% N ₂ , 50% CO ₂	10-15	-	HNO ₃ oxidized + Ca by IW	10.7	640
M	0.5% H ₂ S, 49.5% N ₂ , 50% CO ₂	-	520	steam activated	6.1	300
N	0.5% H ₂ S, 49.5% N ₂ , 50% CO ₂	10-15	509	HNO ₃ oxidized + Zn by IE	10.4	390
O	0.5% H ₂ S, 49.5% N ₂ , 50% CO ₂	10-15	250	HNO ₃ oxidized + Cu by IE	10.6	350

Table 1 Notes:

- All chars were preoxidized, pyrolyzed and steam activated.
- Reactor temperature = 550°C, inlet gas flow rate = 200 cm³/min, and space velocity = 1700 to 2000 hr⁻¹.
- IE = ion exchange method, and IW = incipient wetness method.

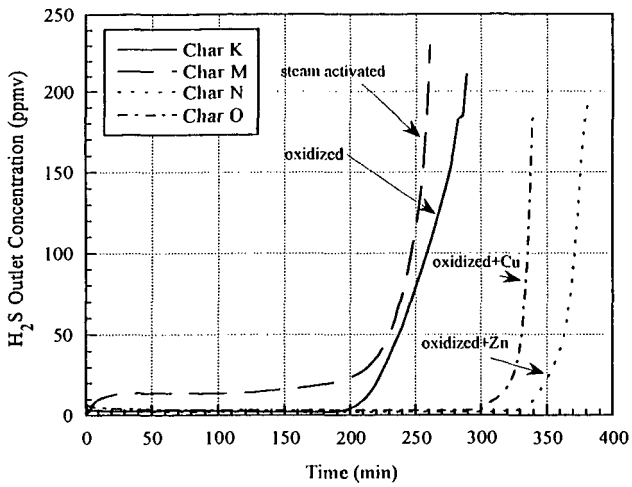


Figure 1. H₂S Breakthrough Curves for Carbon-Based Sorbents using Quartz Reactor

Conditions: SV = 1700-2000 hr⁻¹, 0.5% H₂S, 49.5% N₂, 50% CO₂, 550°C, 1 atm.

METAL IONS REMOVAL FROM WASTEWATER BY ADSORPTION

S. B. LALVANI, T. WILTOWSKI AND A. WESTON*

Department of Mechanical Engineering and Energy Processes
*Department of Engineering Technology
Southern Illinois University
Carbondale IL 62901

ABSTRACT

Three different carbonaceous adsorbents consisting of (i) commercially available lignin (L); (ii) carbon soot produced by arc evaporation of graphite rods (AC); and (iii) commercially available carbon (RC) were employed for the removal of hexavalent and trivalent chromium, and the cations of lead and zinc. AC carbon was found to selectively adsorb only the hexavalent form of chromium which exists as a number of anionic species in the water. Insignificant metal cation adsorption was observed with AC. However, lignin is found to adsorb all the metal ions employed in the study. RC used in this investigation adsorbs only the metal cations and does not remove the hexavalent form of chromium used. Equilibrium as well as kinetic data obtained are analyzed in light of a mathematical model developed which assumes that the overall metal removal rate is controlled by the rate of mass transport of solute from bulk to the surface of the adsorbent.

INTRODUCTION

The presence of heavy metals in the environment is a major concern due to their toxicity to many life forms. Unlike organic pollutants, the majority of which are susceptible to biological degradation, heavy metals will not degrade into harmless end products. Thus, treatment of aqueous wastes containing soluble heavy metals requires concentrations of the metals into smaller volume followed by recovery or secure disposal. Heavy metals can be found in a variety of industries, in particular mining, metal processing, finishing and plating. Effluents from these industries contain heavy metals, the concentrations of which are regulated by governmental agencies. Thus, it is often required to remove heavy metals before discharge of various effluents. The major techniques employed for heavy metal removal from industrial wastewaters include precipitation, reduction, ion-exchange, and adsorption. Attempts have been made by several researchers to develop alternate inexpensive methods for heavy metal removal using industrial waste materials (discarded tires, fly ash, sludge), agricultural products, and byproducts (starch, tree barks, onion skin, coconut shell, palm pressed fibers, lignin), and naturally occurring minerals (coal, peat moss, pyrite).

The choice of adsorbents used in this study was motivated by the following rationale. Lignin, an inexpensive naturally occurring material is a component of woody biomass. It is available in large quantities as a byproduct from the paper and pulp industry. Lignin contains many oxygen functionalities such as phenols and ketones which can serve as adsorption sites for binding heavy metals. Carbon produced from graphite rods by electrical arcing method under inert atmosphere is expected to have unusual properties. The carbon soot produced under these conditions also leads to fullerene formation. A commercially available activated carbon (RC) was used as a control to compare the metal removal properties of lignin (L) and the carbon produced by arc evaporation of graphite rods (AC).

EXPERIMENTAL METHODS

Lignin was obtained from Westvaco Corporation. It is characterized as Indulin AT, a purified powder form of kraft lignin, which is completely free of all hemicellulosic materials. The arc-assisted synthesis of carbons (AC) is reported in a previous paper(1). The method involves arcing of graphite electrodes under flowing helium atmosphere. The alternating current applied to the electrodes ranged from 100-160 amperes. The application of this high current resulted in vaporization of the graphite. The condensed soot was collected and used as an adsorbent. In addition, a commercially available activated carbon (RC), Darco TRS obtained from American Norit Company was also used as an adsorbent for the metal ion removal from aqueous solutions.

Batch sorption experiments were conducted at a constant room temperature of 25 °C using a 500 ml Erlenmeyer flask. The stirred reaction mixture consisted of a total volume of 250 ml. When necessary, the initial pH of the solution was adjusted. The metal concentration was determined by inductively-coupled plasma spectroscopy (ICP).

RESULTS AND DISCUSSION

The effect of initial chromium concentration on the removal of hexavalent chromium at solution pH (initial) of 4.5 using the arc assisted produced carbon (AC) is shown in Figure 1. The adsorbent loading used was 5 g/l and the experiments were conducted for a period of 24 h. The chromium removal (%) is found to increase with the initial metal concentration reaching a maximum value of approximately 94%, however, with a further increase in metal concentration, the removal is found to decrease. Similar albeit lower hexavalent chromium removal vs. concentration trends are observed when lignin is used as an adsorbent in the metal ion containing solution prepared at an initial pH value of 2.5 (Figure 1). Up to 53% metal removal was observed in the case of lignin. It must be noted that when the commercially available activated carbon (RC) was used very small amount of hexavalent chromium removal was obtained. For example, the use of initial metal concentration of 20 ppm in experiments conducted at three different initial pH values of 2.5, 3.0 and 4.5 resulted in 24.6, 14.0, and 9.1% chromium removal, respectively. The data reported in Figure 1 were used to prepare adsorption isotherms. AC adsorbent does not seem to follow either Langmuir or Freundlich isotherm models. The maximum adsorption capacity for the Cr^{6+}/AC system was found to be 8.9 mg/g of sorbent. On the contrary, data for the $\text{Cr}^{6+}/\text{lignin}$ system represents a relatively good fit to the Langmuir equation and can be expressed by the following equation:

$A^{-1} = 2.9 \cdot C_e^{-1} + 0.18$, where A is the adsorption capacity and C_e is the equilibrium concentration in mg/l. The maximum adsorption capacity is estimated to be 5.64 mg/g of sorbent.

The data on removal of trivalent chromium at an initial pH value of 3.0 as function of the metal concentration for the three adsorbents are shown in Figure 2. Experiments were conducted for 24 h using 5 g/l of adsorbent loading. RC adsorbent is found to remove practically all the metal present in the solution. In the case of lignin, about 90% metal removal is observed at low metal ion concentrations. However, an increase in metal concentration results in corresponding lower removal (%). On the other hand, essentially no trivalent chromium removal is noted when the arc-assisted produced carbon (AC) was used in these experiments.

In the experiments involving metal cations of lead and zinc, practically no metal removal was observed when the arc-assisted produced carbon (AC) was used especially at low pH values. For example, in the case of experiments involving lead (Pb^{2+}), 0, 2 and 25% metal removal was noted at pH values of 3.0, 4.5 and 9.0 respectively. RC carbon was observed to remove 100% lead at pH values ranging from 2 to 9.5. Lignin also showed a great affinity for lead. The metal removal (%) increases with pH. For example, the removal of lead by lignin is 47, 74 and 98% at pH values of 2.0, 2.5 and 3.0 respectively. Both, RC and lignin showed 100% zinc removal while no metal removal was observed for AC up to a pH value of 6.0. AC showed about 30% zinc removal at a pH value of 9.0.

The data obtained above can be explained as below. Hexavalent chromium is present in aqueous solutions mainly as anionic chromate species. Therefore, AC carbon is capable of removing this form of chromium as it is hypothesized to contain positive charge on the surface. It must be noted that this carbon is produced by arc evaporation of graphite rods in the absence of air or oxygen. This hypothesis also explains the inability of this form of carbon to remove cations of chromium, lead and zinc at relatively low pH values. At high pH values the surface charges of AC are neutralized, therefore it is able to adsorb limited amount of metal cations. Lignin contains mainly oxygen functionalities, therefore it is able to remove metal cations in addition to the anionic chromate species. On the other hand, RC is activated using steam or air, therefore its surface has mainly oxygen functionalities which serve as negatively charged sites for binding only the metal cations.

REFERENCES

1. Weston, A. and Murthy, M., "Synthesis of Fullerenes: An Effort to Optimize Process Parameters," Carbon, 34, 10, 1267-1274, 1996.

Figure 1. Hexavalent Chromium Removal vs. Concentration

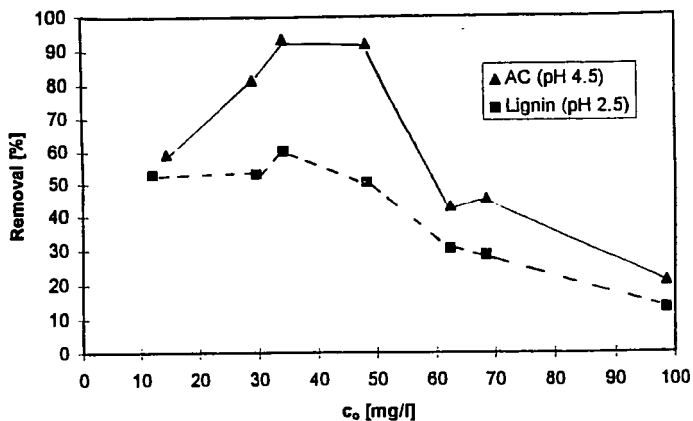


Figure 2. Trivalent Chromium Removal vs. Concentration

